Contract N00014-86-K-0753

Development of Metastable Processing Paths

for

High Temperature Alloys

Semi-Annual Technical Report
submitted to
Defense Advanced Research Projects Agency (DoD)
for the period
April 1, 1988 through September 30, 1988

Contractor: Metallurgy Division
National Institute of Standards and Technology
Gaithersburg, MD

Principal Investigator: William J. Boettinger
301-975-6160

Senior Project Scientists: Leonid A. Bendersky
John W. Cahn
Ursula R. Kattner

Effective Date of Contract: February 9, 1987

Contract Expiration Date: December 31, 1989

Amount of Contract: $600,000

ARPA Order Number: 6065

Program Code Number: 7D10

Table of Contents

Summary

The possibility of developing new processing strategies for high temperature intermetallic compounds is being investigated. In particular rapid solidification followed by controlled heat treatment may provide new and unusual microstructures of multiphase materials. This report describes research performed at NIST to develop predictive models for solubility extension and metastable phase formation of intermetallic compounds and research to improve the phase diagram modeling of systems involving ordered phases.

Theory has been developed to predict the formation of disordered form of intermetallic compounds during rapid solidification. Using a modification of the Aziz solute trapping theory, solidification velocities required to form, for example, a BCC phase from the melt when a B2 phase is the stable phase have been developed. In the present reporting period, this theory has been extended to the case where a FCC phase replaces a $L1_0$ phase.

Experimental research has continued on the intermetallic system, NiAl-NiTi, using laser surface melting and examination by transmission electron microscopy. In the NiAl-NiTi system, the equilibrium intermediate Heusler phase, Ni_2AlTi, was suppressed by rapid solidification and extension of the composition range of the NiAl and NiTi phases was observed by melt spinning. To quantify the solidification rates required for this process, samples have been prepared by pulsed laser melting where the solidification rate can be varied between 1-10 m/s. Preliminary experiments show the formation of the B2 phase at the Ni_2AlTi composition, which under equilibrium processing forms the $L2_1$ structure.

Experimental work on ternary alloys surrounding the composition Ti_2NbAl

to determine the phases present in arc melted and heat treated samples has continued. TEM investigations are required to sort out the complex ordering reactions in this important alloy system. A broad equilibrium composition range for the B2 phase has been identified at 1100°C and complex low temperature (~700°C) transitions are being examined.

An evaluation of existing data and a thermodynamic calculation of the Ti-Al-Ta phase diagram has been initiated using the THERMOCALC code. This activity was requested at the March 1988 review of the DARPA/ONR Program on "Development of High Temperature Intermetallics for Structural Aerospace Applications" at Pratt & Whitney, Florida.

I. Introduction

The development of high temperature materials is closely related to the formulation of processing strategies for chemically ordered phases. Most intermetallic compounds including aluminides, carbides, and silicides as well as high temperature ceramic phases are ordered. However, optimum mechanical properties are likely to come from intimate dispersions of several phases, some of which are ordered. These dispersions can be produced by a phase transformation sequence involving both ordering and phase separation, beginning with a solid phase of a carefully selected unstable composition made by rapid solidification.

Recently, significant advances have occurred in the utilization and understanding of rapid solidification processing of alloys. Factors which promote refined segregation, solubility extension and metastable phase formation have been identified. However, much of this research has been focused towards disordered crystalline phases: i.e., terminal solid solutions, not ordered intermetallic compounds.

At the same time, significant advances have been realized in the thermodynamics and kinetics of order-disorder transitions. The distinction between first and higher order transitions has been clarified, the kinetics of ordering reactions and the structure and mobility of APB's have been determined and reactions that involve fine scale ordering and compositional separation have been studied.

This research attempts to combine the advances in these areas to develop new processing strategies for high temperature ordered multiphase materials.

In section II of this report we describe theoretical and experimental research focused on determining the possibility of extending the solubility range of ordered phases by rapid solidification. Subsequent heat treatment of these metastable alloys can form stable high temperature multiphase mixtures. This research also includes an examination of the state of nonequilibrium order of rapidly quenched intermetallic compounds.

Section III of this report summarizes research at phase identification in composition surrounding Ti_2NbAl.

Section IV of this report describes phase diagram activities involving ordered phases. A preliminary calculation of the ternary diagram Ti-Ta-Al has been produced.

II. Solubility Extension and Disordering of Intermetallic Compounds by Rapid Solidification

(a) Theory of Solute & Disorder Trapping by Rapid Solidification

A model has been developed to predict the long range order parameter and composition of a chemically ordered phase as a function of interface velocity. The details of this model were described in the previous semi-annual report. The model is an extension of the solute trapping model of

Aziz and relies on an analysis of the interdiffusion across the liquid solid interface between a liquid phase and a solid composed of two sublattices. The model predicts the transition from solidification of a solid phase with equilibrium long range order parameter and with equilibrium partitioning of composition at low interface velocity to solidification of a disordered crystalline solid with the same composition as the liquid at high solidification velocity.

A broad range of experimental results on rapid solidification of intermetallic compounds suggests that solute trapping and disorder trapping do not occur for line compounds under melt spinning conditions. Trapping seems only to occur for ordered phases in which the ordering is not so strong; i.e., where the equilibrium composition range is large (~10%). The general theory was explored and a simple result related to this point has been obtained. The critical velocity for the trapping of disorder, V_C; i.e., the velocity above which only the disordered variant of the intermetallic compound can form can be estimated from

$$V_C \simeq V_D\left(\frac{T_C}{T_m} - 1\right)$$

where V_D is the ratio of the interface diffusivity to the jump distance (~10^2 cm/s), T_C is the critical temperature for the order-disorder transition, and T_m is the melting point of the compound. When the compound is ordered up to its melting point $T_C/T_m > 1$. One can see that the higher T_C, which relates directly to the strength of the ordering, the higher the velocity required to trap disorder. For line compounds $T_C >> T_m$ and thus V_C may be unattainable in normal rapid solidification methods.

The results of this theory have been calculated for solids which have first and second order ordering transitions during the current reporting

period. Discontinuities in both order parameter and solid composition occur when the growth velocity is increased when the equilibrium ordering reaction is first order. These results are described in detail in the preprint enclosed in the appendix.

(b) NiAl-NiTi Alloys

In previous reports experimental research on the microstructure of melt spun alloys in the NiAl-NiTi system was described. Eutectic alloys of NiAl-Ni_2TiAl and Ni_2TiAl-NiTi solidified as a single B2 phase. However, results on alloys with composition Ni_2TiAl were not clear. The APB size was sufficiently coarse that the non-equilibrium solidification product could not be determined with certainty. In collaboration with Professor Mike Aziz of Harvard we have performed pico-second pulse melting. This technique produces solidification rates of 1-5 m/s. Initial results show that extremely fine $L2_1$ domains are produced by this technique suggesting that the solidification process produced the B2 phase with subsequent solid state ordering to the $L2_1$ structure. Future experiments with this method will permit testing of the theory described in the previous section.

III. B2 and Related Phases in the Ti-Al-Nb System

Titanium aluminides (Ti_3Al and TiAl) with ~10 at% Nb additions have received considerable attention as potential low density, high strength and creep resistant materials. However, the phase equilibria in this ternary system is poorly understood. Because the presence of BCC-based phases in these alloys seems to play an important role in the deformation, in-depth studies of the BCC-based phase fields are being conducted. A series of alloys surrounding the composition Ti_2AlNb are being studied by TEM to determine the structure of phases present in arc cast, melt spun and heat

treated samples. When complete, these results, combined with those from the University of Wisconsin by J. Perepezko and Y. A. Chang under DARPA sponsorship, will be combined with ternary phase diagram calculations performed under this contract to determine the ternary phase diagrams Ti-Nb-Al.

(a) Literature Survey

Experimental work focused on ternary equilibria in the BCC field of the Ti-Al-Nb system is sparce. Strychor, Williams and Soffa (Met. Trans 19A (1988) 225) have shown that alloys with ~25 at% Al and between 7 and 20 at% Nb which are quenched from 1250°C are single phase B2 with APB's. This indicates that the BCC to B2 transition for these compositions occurs below 1250°C. Quenched alloys with 0-7 at% Nb are HCP α' martensite. The B2 alloys also contain a tweed structure of ordered ω phase. During aging at 400°C for 100 hours, the B2 phase was partially consumed by an ordered ω phase. Evidence for additional ordering of ω into a $B8_2$ (Zr_2Al) phase is also presented. No DO_{19} phase was observed to form for alloys with greater than 7 at% Nb.

Banerjee, Gogia, Nandi and Joshi (Acta Met. 36 (1988) 871) have studied the composition Ti-25 at% Al-12.5 at% Al. Alloys held at 1100°C for 3 hours and quenched contain $\alpha_2(DO_{19})$ and B2 phases. The B2 phase contains no APB's. This indicates the equilibria at 1100°C is DO_{19} + B2, not DO_{19} + BCC. Furnace cooling of this structure yields microstructures that suggest that both of the phases transform partially to an orthorhombic O(Cd_3Er) phase with symmetry Cmcm. Evidence is presented that $\alpha_2 \rightarrow \alpha_2$ + O by simultaneous ordering and spinodal decomposition and that the B2 phase also transforms by nucleation and growth to the orthorhombic phase. They also infer that the

orthorhombic phase has a preferred stoichiometry of Ti_2NbAl.

Banerjee, Nandy and Gogia (Scripta Met. 21 (1987) 597) have examined the site occupancy of the B2 phase which occurs in a two-phase mixture with the α_2 phase in heat treated samples (no temperature given) of Ti-25.6 at% Al-10.1 at% Nb. Using channeling enhanced microanalysis they determined that one sublattice was mostly Ti while the other contained the excess Ti and the Al and Nb atoms. Using site fractions x_I^j, they give

$$\begin{vmatrix} x^{\alpha}_{Ti} & x^{\alpha}_{Al} & x^{\alpha}_{Nb} \\ x^{\beta}_{Ti} & x^{\beta}_{Al} & x^{\beta}_{Nb} \end{vmatrix} = \begin{vmatrix} .96 & 0 & .04 \\ .28 & .48 & .24 \end{vmatrix} .$$

(b) Experimental Procedure

Alloys shown in Table 1 were prepared by arc melting. In excess of ten remelts were necessary to homogenize the buttons.

Table 1. Ti-Al-Nb Alloys Under Investigation

Ingot #	at% Ti	at% Al	at% Nb	ppm O	ppm N	ppm H
30	50 (51.1)	25 (23.9)	25 (25.0)	500	130	22
01	50 (50.6)	12.5 (12.2)	37.5 (37.2)	500	320	34
02	37.5 (38.1)	25 (24.3)	37.5 (37.6)	290	30	7
03	62.5 (63.5)	25 (24.2)	12.5 (12.3)	520	90	12
04	50 (51.4)	37.5 (36.2)	12.5 (12.4)	630	50	7

Cast structures were homogenized with a 3 hour heat treatment at 1400°C in a vacuum-tight furnace under 2/3 atm gettered Argon. It was found necessary to rest samples on a Y_2O_3 coated Al_2O_3 substrate to prevent reaction with Al_2O_3. Cooling was performed by lowering the samples out of the hot zone of the furnace into a lower chamber. The cooling rate was estimated by visual observation and by measurements of the furnace vendor to be ~400 K/min. Heat treatments at 1100°C were performed after the 1400°C treatment by lowering the furnace temperature. Equilibration at 1100°C occurred in ~5 min. Heat treatments at 700°C were performed by sealing

individual samples from the 1400°C treatment in quartz tubes. Samples were wrapped in Ta foil and tubes were backfilled with 2/3 atm He.

Chemical analysis was performed on the samples homogenized at 1400°C. Because these samples were nominally single phase when viewed by optical or SEM metallography, microprobe analysis with elemental standards yields reliable analysis of the bulk alloy compositions. The values obtained are given in parentheses in Table 1. Oxygen, nitrogen and hydrogen analysis was performed on these samples by a commercial vendor and is also given in Table 1.

(c) Results

The results of microstructural investigation of phase identification to date are summarized in Table 2. Considerable solid state transformation occurs during cooling in some samples. Actual phases present are listed along with the inferred equilibrium at temperature and the decomposition path. The results combine observations made by optical metallography, x-ray diffraction and electron microscopy.

Microstructure of Arc Melted Buttons - Optical metallography of the as-cast buttons revealed dendritic but single phase structures in all samples except #03. Microsegregation was small (<1%) but the cores of the dendrites were rich in Nb as judged from backscatter contrast. Observation of grain boundaries cutting across dendrite arms suggests significant grain coarsening (up to 300 μm) during solid state cooling. In sample #03, a fine martensitic plate structure was visible. X-ray diffraction indicated the structure to be DO_{19} (Ti_3Al).

Microstructure of Samples Heat Treated at 1400°C - Optical metallography of the samples cooled from 1400°C reveals the absence of dendritic

Table 2 - Summary of Phase Analysis in Ti-Al-Nb Alloys

HEAT TREATMENT	OBSERVATION METHOD	ALLOY				
		3	4	30	1	2
CAST	OPTICAL	NONDENDRITIC FINE PLATES MARTENSITE?	SINGLE PHASE DENDRITIC	SINGLE PHASE DENDRITIC	SINGLE PHASE DENDRITIC	SINGLE PHASE DENDRITIC
	X-RAY	D019				
	MICROPROBE		DENDRITE CORES NB RICH	DENDRITE CORES NB RICH	DENDRITE CORES NB RICH	DENDRITE CORES NB RICH
	TEM					
	INFERRED PATH	L to BCC BCC to D019	L to BCC	L to BCC	L to BCC	L to BCC
1400 C 3 HRS COOLED ~400 C/min	OPTICAL	FINE PLATE STRUCTURE	SINGLE PHASE LARGE EQUIAXED GRAINS PPTS ?	SINGLE PHASE LARGE EQUIAXED GRAINS PPTS ?	SINGLE PHASE LARGE EQUIAXED GRAINS	SINGLE PHASE LARGE EQUIAXED GRAINS
	X-RAY					
	MICROPROBE					
	TEM	D019 PLATES with APBS VARIANTS RELATED TO BCC	ORDERED OMEGA or B82	B2 with minor fraction of twinned D019	BCC with faint B2 reflections	B2
	INFERRED EQUILIBRIUM AT 1400 C	BCC	BCC or B2	BCC or B2	BCCor B2	BCC or B2
	INFERRED PATH	BCC to B2 B2 to D019	BCC to B2 B2 to OR OMEGA or B82	BCC to B2 ppt. of D019	BCC to B2	BCC to B2
1400 C 3 HRS 1100 C 4 DAYS COOLED ~400 C/min	OPTICAL	FINE PLATE STRUCTURE	LARGE EQUIAXED GRAINS LARGE PPTS. ON GRAIN BOUND. AND INTERIOR	SMALL GRAINS WITH G.B. PPTS.	SINGLE PHASE LARGE EQUIAXED GRAINS	LARGE EQUIAXED GRAINS LARGE PPTS. ON GRAIN BOUND. AND INTERIOR
	X-RAY					
	MICROPROBE					
	TEM	D019 PLATES with APBS VARIANTS RELATED TO BCC	ORDERED OMEGA or B82 MATRIX WITH D019 PPTS.	B2 with minor fraction of twinned D019	BCC with faint B2 reflections	B2 MATRIX LARGE SIGMA PPTS.
	INFERRED EQUILIBRIUM AT 1100 C	BCC or B2	B2 + D019	B2	BCC or B2	B2 + SIGMA (Nb2Al)
	INFERRED PATH	B2 to D019	B2 to ORDERED OMEGA or B82	precipitation of D019	.....	.....

microsegregation and very coarse grains (~2 mm). The microstructures appear essentially featureless with the exception of #03 which is martensitic. TEM examination of the martensitic sample indicates complete transformation from the high temperature phase which existed at 1400°C to a DO_{19} martensite. The other four compositions consist primarily of a B2 or related phase. Although no APB's were observed, previous research by Banerjee et al. and Strychor et al. suggest a BCC → B2 ordering occurs ~1200°C. We thus infer that the equilibrium phase at 1400°C is BCC for all five alloys. However, the possibility exists that for some compositions the B2 is stable at 1400°C. High temperature x-ray diffraction will be used to answer this point.

Besides the B2 ordering which occurs during cooling, sample #04 completely transforms to ordered ω (or possible $B8_2$). Sample #30 contains small plates of twinned DO_{19}.

Microstructure of Samples Heat Treated at 1100°C for Four Days - The microstructure of samples #03, #30, and #01 cooled from 1100°C are identical to those cooled from 1400°C. Oddly the result for #03, that the phase present at 1100°C after 3 hours is B2, directly contradicts the result of Banerjee et al. who found B2 + DO_{19} under these conditions. This may be related to differences in cooling rate.

Sample #02 contained B2 and σ phases while sample #04 contained B2 + DO_{19}. The B2 in this alloy #04 was completely transformed to ordered ω.

(d) Future Research

Future work will involve an analysis of the phases present at 700°C after a one month annealing. The calculated ternary phase diagram Ti-Al-Nb which was presented in the last report will be modified to be consistent with this new data and other data generated by J. H. Perepezko and Y. A. Chang at

the University of Wisconsin, Madison, under DARPA sponsorship.

IV. Phase Diagram Modeling

We have undertaken a preliminary calculation of the Ti-Al-Ta ternary system in response to requests by Ralph Hecht, Pratt-Whitney, Florida, for use in their DARPA Program "High Temperature Metallics for Structural Aerospace Applications."

A preliminary calculation of the Ti-Al-Ta ternary phase diagram was undertaken using the THERMOCALC DATABANK system described by B. Sundman, B. Jansson and J. O. Anderson (CALPHAD 9, 2 (1985) pp. 153-190). The stability ranges were adjusted to match the isothermal section at 1100°C by Sridharan and Nowotny (Z. Metallkunde 74 (1983) 468).

In the calculations of the binary systems the liquid and elemental phases were described as sub-regular solutions. The intermetallic compounds in the Ta-Al and Ti-Al were described with the Wagner-Schottky model, where intermetallic compounds are considered to consist of different sublattices allowing substitutional solutions on each of these sublattices. Since the Wagner-Schottky model is mathematically a special case of the sublattice model, the parameters of these intermetallic compounds can be easily transformed to the sublattice model description of the THERMOCALC DATABANK system. For the present only the σ and $TaAl_3$ intermetallics were modeled in the Ta-Al binary.

For the extrapolation of ternary Ti-Ta-Al system all phases must be allowed to have ternary ranges of homogeneity, which means for the Wagner-Schottky phase that they have to be modeled as metastable phases for the two other binary systems.

As a first approximation the Gibbs energies of formation of the Ta-Al

compounds in the Ti-Al system and the Ti-Al compounds in the Ta-Al system were assumed to be the same as in the system where these compounds are stable, for the Ta-Ti system the Gibbs energies of formation were assumed to be the same as for these compounds consisting only of Ta or Ti, respectively.

In order to prevent these metastable phases from becoming stable in the binary systems and to adjust the calculated phase diagram to experimental results at 1100°C, the Gibbs free energies of formation of these metastable phases were adjusted by assuming that the entropies of formation of the metastable phases have the same magnitude as the stable phases and the enthalpies of formation of the metastable phases are more positive than those of the stable phases. The ternary ranges of homogeneity at 1100°C calculated with these parameters were acceptable except for the hcp and $L1_0$ phase, where they were too small. This was adjusted by giving the Ta-Al interaction term of the hcp phase the most negative value possible, without the hcp-phase becoming stable in the Ta-Al system. For the $L1_0$-phase ternary interaction terms were introduced between Al and Ta on the first sublattice and with Ti on the second one and between Al and Ti on the first sublattice and Ta on the second one.

The calculated binary diagrams used for the Ti-Ta-Al ternary calculation are shown in Figures 1, 2, and 3. The correct Ti-Al and Ta-Al diagrams are still subject to debate in some regions and can be modified at a later time.

The results obtained from the calculations with these parameters are shown in Figures 4, 5, and 6. Ternary phases were omitted at this initial stage. Figures 4 and 5 show isothermal sections at 1100, and 1400°C, while Figure 6 shows the liquidus projection.

Further work on phase diagram modeling in this system must await a more

precise definition of the measured phase boundaries.

V. Fiscal Status

(1) Amount currently provided for contract program

$150,000 for period February 9, 1987 to September 30, 1987.

$200,000 for period October 1, 1987 to September 30, 1988.

(b) Expenditure and commitment during April 1, 1988 to September 30, 1988

$100,000

(c) Estimated funds required to complete this work

October to December 1988	$50,000
January to March 1989	$50,000
April to June 1989	$50,000
July to September 1989	$50,000
October to December 1989	$50,000

Figure Captions

Figure 1. Calculated Ti-Al phase diagram used for calculation of Ti-Al-Ta ternary diagram.

Figure 2. Calculated Ti-Ta phase diagram used for calculation of Ti-Al-Ta ternary diagram.

Figure 3. Calculated Ta-Al phase diagram used for calculation of Ti-Al-Ta ternary diagram.

Figure 4. Calculated isothermal section of the Ti-Al-Ta ternary phase diagram at 100°C omitting ternary phases.

Figure 5. Calculated isothermal section of the Ti-Al-Ta ternary phase diagram at 1400°C omitting ternary phases.

Figure 6. Calculated liquidus and solidus invariants of the Ti-Al-Ta ternary phase diagram omitting ternary phases (liquidus invariants have double arrows).

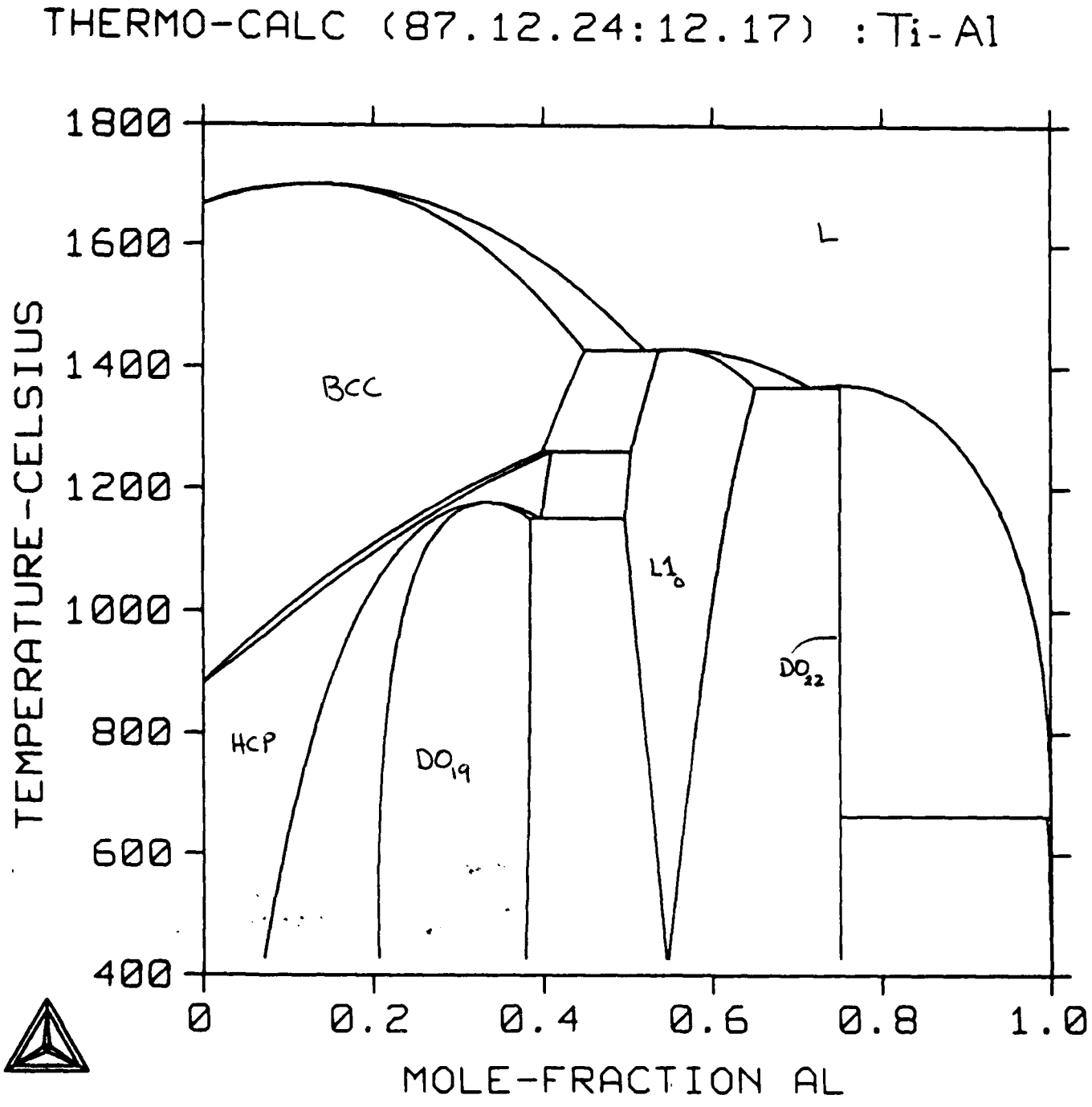
THERMO-CALC (87.12.24:12.17) : Ti-Al
TEMPERATURE-CELSIUS
1800
1600
1400
1200
1000
800
600
400
0
0.2
0.4
0.6
0.8
1.0
MOLE-FRACTION AL
L
BCC
HCP
DO19
L10
DO22

FIG 1

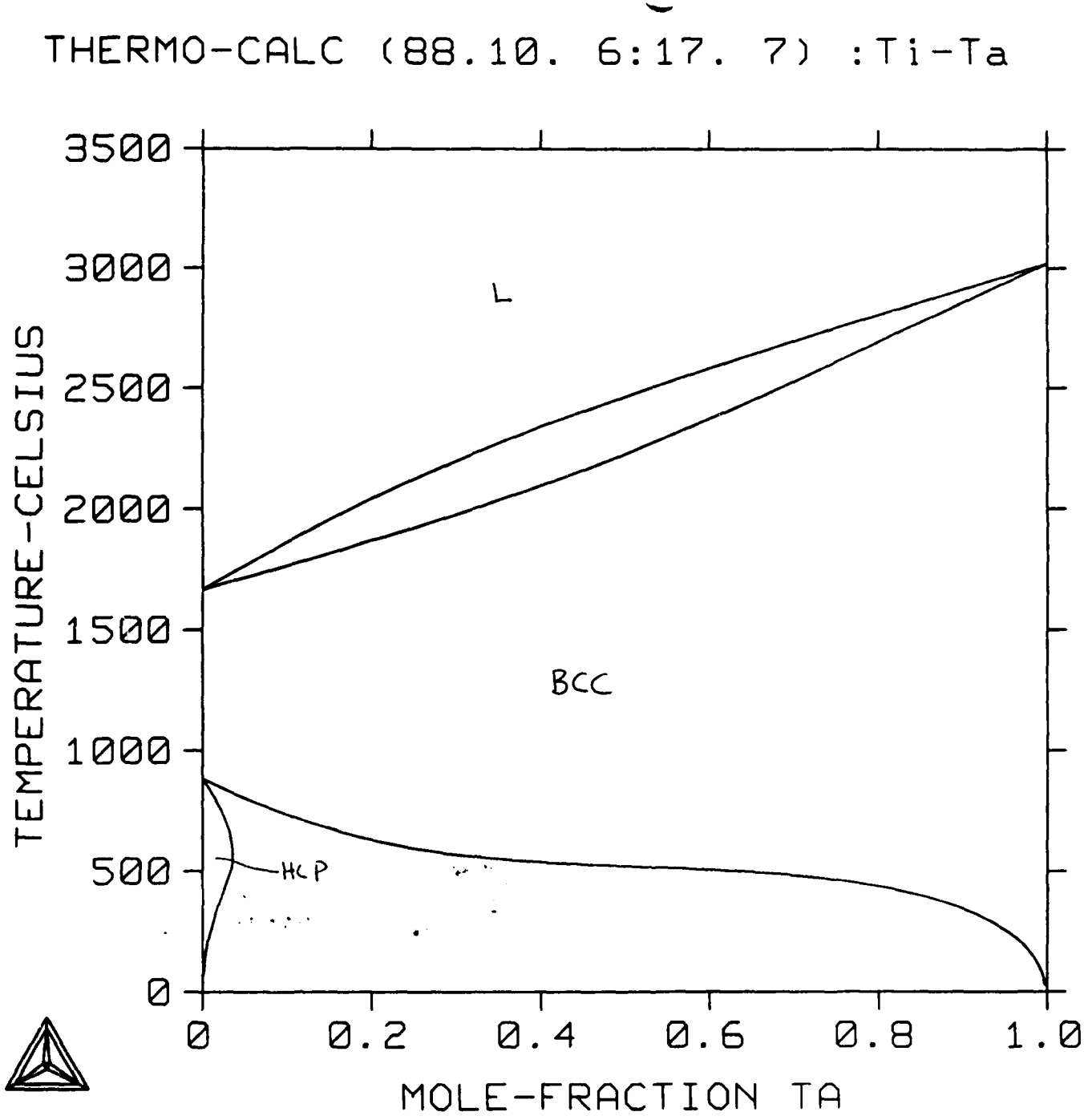
THERMO-CALC (88.10. 6:17. 7) :Ti-Ta
TEMPERATURE-CELSIUS
3500
3000
2500
2000
1500
1000
500
0
L
BCC
HCP
0
0.2
0.4
0.6
0.8
1.0
MOLE-FRACTION TA

FIG 2

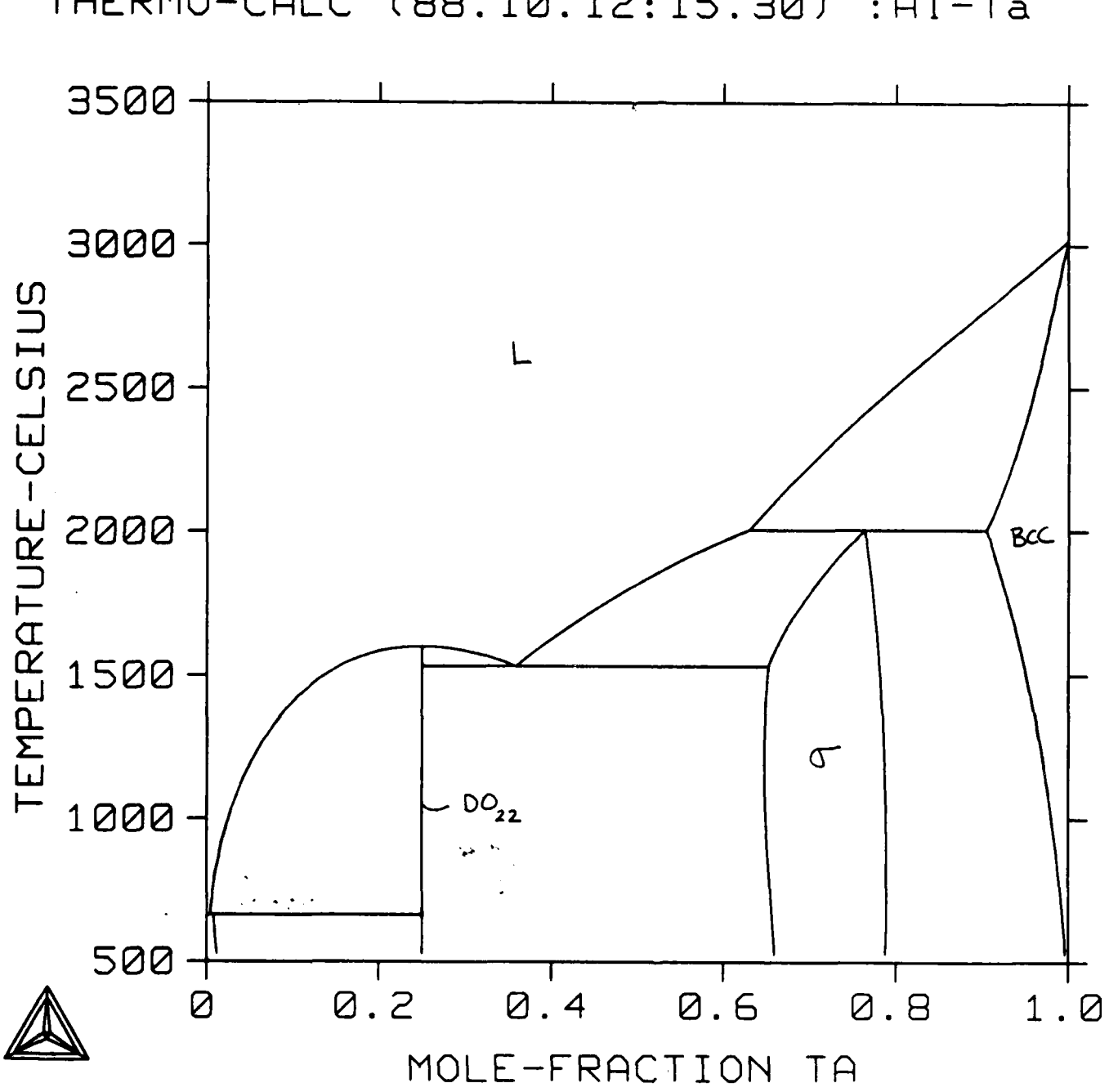
THERMO-CALC (88.10.12:15.30) :Al-Ta
TEMPERATURE-CELSIUS
3500
3000
2500
2000
1500
1000
500
0
0.2
0.4
0.6
0.8
1.0
MOLE-FRACTION TA
L
BCC
σ
DO22

FIG 3

THERMO-CALC (88.10.12:17.25) :Al-Ta-Ti 1100 C

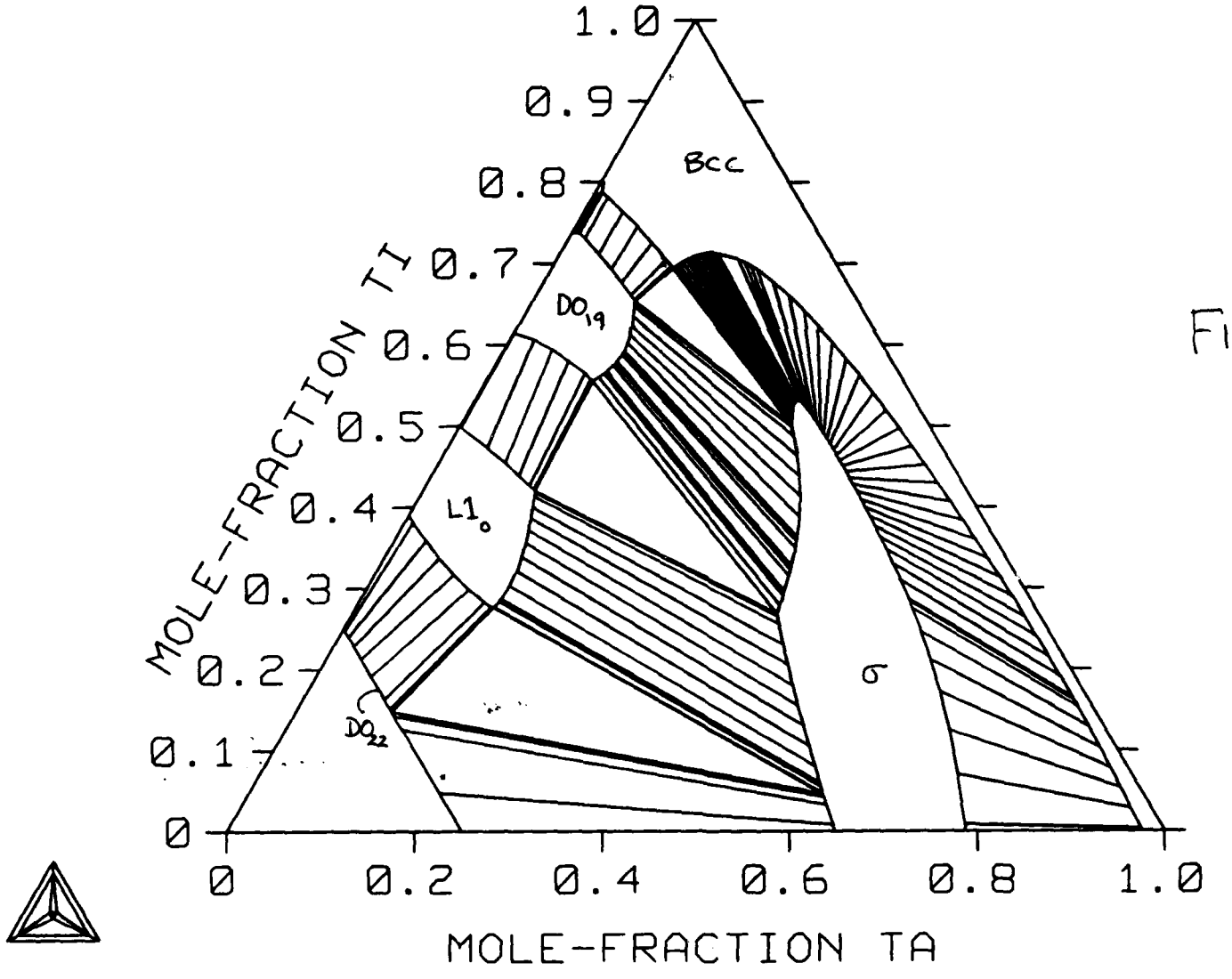

FIG 4

THERMO-CALC (88.10.13:11.55) :Al-Ta-Ti 1400 C

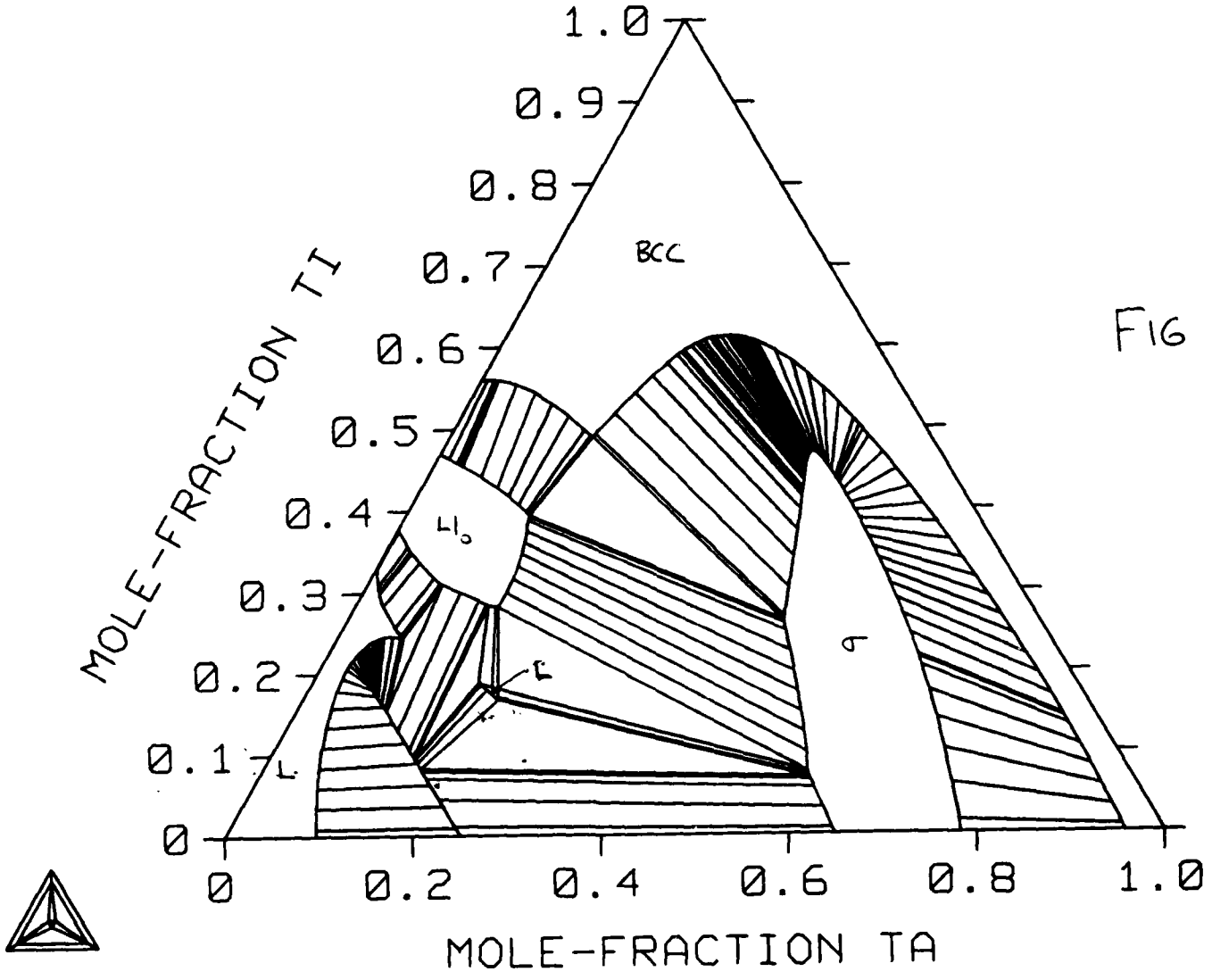

FIG 5

THERMO-CALC (88.10.13:13. 7) :Al-Ta-Ti Liquidus

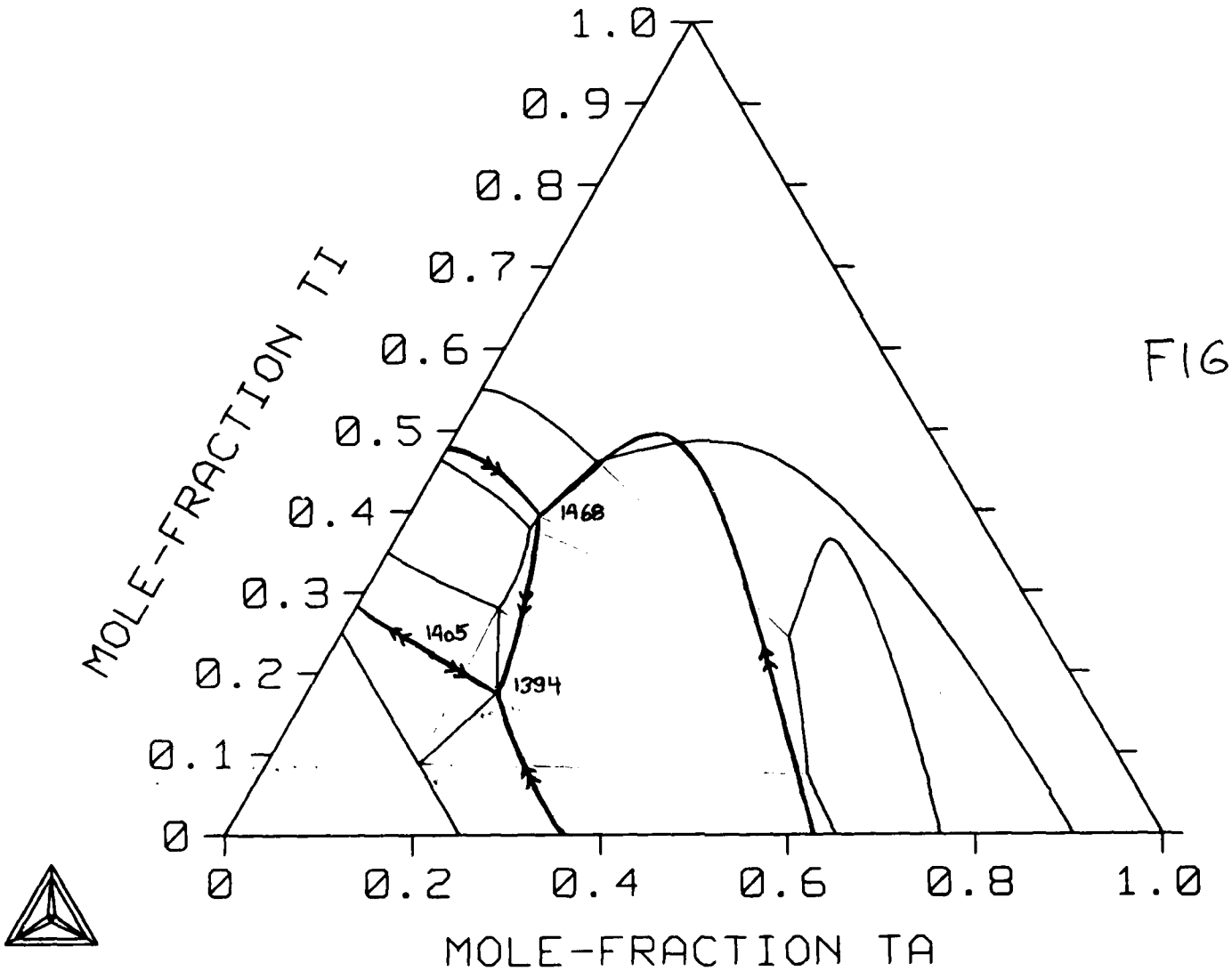

FIG 6

APPENDIX

A Theory for the Trapping of Disorder and Solute in Intermetallic Phases by Rapid Solidification

William J. Boettinger
Metallurgy Division
National Institute for Standards and Technology
(formerly National Bureau of Standards)
Gaithersburg, MD 20899

and

Michael J. Aziz
Division of Applied Sciences
Harvard University
Cambridge, MA 02138

A theory is developed to predict the long range order parameter, composition and interfacial temperature of a chemically ordered phase as a function of interface velocity during rapid crystal growth. The theory extends the solute trapping theory of Aziz to a solid phase consisting of two sublattices. The engulfment of atoms randomly on the two sublattices by the rapidly moving interface is balanced against the interdiffusion across the liquid–solid interface which attempts to restore local equilibrium. With increasing interface velocity the theory predicts a transition from the solidification of a phase with equilibrium long range order parameter and with equilibrium solute partitioning to the solidification of a disordered crystalline phase with the same composition as the liquid. Predictions for various free energy functions for the solid phase suggest that the decrease of order parameter with increasing interface velocity may be continuous or discontinuous and that transitions to solute trapping and to disorder trapping can occur at different growth rates.

1. Introduction

Over the years, considerable attention has been paid to the kinetics of motion of the interface separating two phases, especially to the kinetics of solidification of a melt.

Recent interest in the rapid solidification processing of alloys and other materials using transformations far from equilibrium has renewed interest in these kinetics. Theories of nonequilibrium incorporation of solute into rapidly growing crystals (1–9) are currently the focus of experimental tests (10,11). An interesting additional possibility occurs for intermetallic compounds or other crystals with long range chemical order. Rapid growth can also cause the formation of crystals with nonequilibrium long range order. Because ordering in the solid state during post–solidification cooling can mask events at the liquid–solid interface quantitative experiments to measure the state of long–range order of the solidifying material are difficult to design. However, the observation of solidified phases with high densities of antiphase domains when the phase is normally ordered to the melting point is a clear indication that disorder has been trapped by the process of rapid solidification (12–15).

Kinetic theories for trapping generally fall into two categories: diffuse interface and chemical reaction rate theories. Diffuse interface theories (16–17) solve the Cahn–Hilliard Equation in a moving frame and predict in a formal way that certain kinds of disorder can be induced into a growing phase by rapid interface motion. Chernov has developed a chemical reaction–rate theory that has been applied to both solute trapping during rapid solidification of disordered solid solutions and disorder trapping during solidification of stoichiometric compounds (18). Analytic and Monte–Carlo models of solute trapping based on very similar principles to Chernov's have been developed by others (19–22). Probabilities are assigned for each species to hop into or out of the crystal based on the temperature and the chemical (and structural, e.g., location at a kink) environment; the net hopping rates are summed to yield the growth velocity. In the language of the thermodynamics of irreversible processes, the flux of each species across the interface is a function of the conjugate driving force (chemical potential difference across the interface)

for that species only, being independent of the driving force for the other species. According to these models, for the impurity to be incorporated into a high–energy site (the wrong sublattice in disorder trapping; any lattice site in solute trapping), it must actively hop into it.

The main innovation in the approach of Aziz (1) is that if the impurity does nothing it may end up on a high–energy site by virtue of the formation by its neighbors of a regular lattice around it. Hence to avoid incorporation onto a high–energy lattice site, an atom must diffuse away. (For growth of compounds some of the atoms, of course, will by chance be incorporated onto the right sublattice even if they do no hopping.) Since the maximum speed of diffusion can be rather slow compared to the speed with which crystal–melt interfaces have been observed to move (23–25), the atom may be trapped on a high–energy site by a rapidly moving interface. This implies a strong cross–coupling between the fluxes and driving forces of the individual species (26). These assumptions have been shown experimentally to be much more reasonable, at least for solute trapping during rapid solidification (10–11), than that requiring each atom to actively hop into its final site in the crystal.

In this paper we develop a chemical reaction rate theory for the kinetics of crystallization of an ordered phase at an atomically "rough" interface; i.e., there are no special sites such as ledges or kinks. The interface temperature, composition and order parameter of the solid will be described as functions of the interface velocity and liquid composition at the interface. It is the first theory to treat the simultaneous trapping of solute and disorder. This is carried out by modeling solute trapping of the undesirable species on each sublattice. The mean of the sublattice compositions yields the overall solid composition; their difference yields the order parameter. First, the conditions for equilibrium between a liquid and a solid phase consisting of two equivalent sublattices are

developed in a form required for the kinetic theory. Second, the kinetic theory is presented; and third, numerical results for the growth of solid phases with first and second order order–disorder transitions are presented.

2. Thermodynamics of the Phases at Equilibrium

We assume for simplicity that the solid phase consists of two equivalent sublattices α and β with no vacancies and that a total free energy function for the solid, G^T is a function of n_i^j, the number of moles of component i (i = A,B) on sublattice j (j = α,β). The constraint of equal number of lattice sites of the two sublattices requires that $n_A^\alpha + n_B^\alpha = n_A^\beta + n_B^\beta$. One can formally define the chemical potential of component i on the j sublattice as

$$\mu_i^j = \frac{\partial G^T}{\partial n_i^j} . \qquad [1]$$

The conditions for equilibrium in the solid phase are given by

$$\mu_B^\alpha - \mu_A^\alpha = \mu_B^\beta - \mu_A^\beta . \qquad [2]$$

If we assume that the constraint on the number of moles on each sublattice also holds in the solid at an interface with a liquid phase then one obtains at equilibrium

$$\begin{aligned} \tfrac{1}{2}(\mu_A^\alpha + \mu_A^\beta) &= \mu_A^L \\ \tfrac{1}{2}(\mu_B^\alpha + \mu_B^\beta) &= \mu_B^L \end{aligned} \qquad [3]$$

where μ_A^L and μ_B^L are the chemical potentials of the liquid phase. As a consequence of [2] and [3], the conditions

$$\begin{aligned} \mu_B^\alpha - \mu_A^\alpha &= \mu_B^L - \mu_A^L \\ \mu_B^\beta - \mu_A^\beta &= \mu_B^L - \mu_A^L \end{aligned} \qquad [4]$$

also hold at equilibrium. These conditions must be satisfied at the zero growth velocity limit of any kinetic theory.

The free energy of the solid phase is usually written on a molar basis, G_m^S, in terms

of the compositions of A and B atoms on the α and β sublattices, x_A^α, x_B^α, x_A^β, x_B^β given by

$$\begin{aligned} x_A^\alpha &= x_A^S + \tfrac{1}{2}\eta \\ x_A^\beta &= x_A^S - \tfrac{1}{2}\eta \\ x_B^\alpha &= x_B^S - \tfrac{1}{2}\eta \\ x_B^\beta &= x_B^S + \tfrac{1}{2}\eta. \end{aligned} \quad [5]$$

The long range order parameter, η is given by

$$\eta = x_A^\alpha - x_A^\beta = x_B^\beta - x_B^\alpha \quad [6]$$

and the solid compositions, x_A^S, x_B^S, are given by

$$\begin{aligned} x_A^S &= \tfrac{1}{2}(x_A^\alpha + x_A^\beta) \\ x_B^S &= \tfrac{1}{2}(x_B^\alpha + x_B^\beta) \end{aligned} \quad [7]$$

where clearly, $x_A^\alpha + x_B^\alpha = 1$, $x_A^\beta + x_B^\beta = 1$, $x_A^S + x_B^S = 1$. With these definitions of composition, the molar free energy G_m^S is given by

$$G_m^S = \tfrac{1}{2}(\mu_A^\alpha x_A^\alpha + \mu_B^\alpha x_B^\alpha + \mu_A^\beta x_A^\beta + \mu_B^\beta x_B^\beta). \quad [8]$$

If G_m^S is treated as a function of independent variables x_B^α and x_B^β then

$$\mu_B^\alpha - \mu_A^\alpha = 2\frac{\partial G_m^S}{\partial x_B^\alpha} \quad [9]$$

$$\mu_B^\beta - \mu_A^\beta = 2\frac{\partial G_m^S}{\partial x_B^\beta} \quad [10]$$

and

$$\tfrac{1}{2}(\mu_A^\alpha + \mu_A^\beta) = G_m^S - x_B^\alpha \frac{\partial G_m^S}{\partial x_B^\alpha} - x_B^\beta \frac{\partial G}{\partial x_B^\beta} \quad [11]$$

$$\tfrac{1}{2}(\mu_B^\alpha + \mu_B^\beta) = G_m^S + (1 - x_B^\alpha)\frac{\partial G_m^S}{\partial x_B^\alpha} + (1 - x_B^\beta)\frac{\partial G_m^S}{\partial x_B^\beta}. \quad [12]$$

If on the other hand independent variables, x_B^S and η, are used

$$\mu_B^\alpha - \mu_A^\alpha = \frac{\partial G_m^S}{\partial x_B^S} - 2\frac{\partial G_m^S}{\partial \eta} \quad [9]$$

$$\mu_B^\beta - \mu_A^\beta = \frac{\partial G_m^S}{\partial x_B^S} + 2\frac{\partial G_m^S}{\partial \eta} \quad [10]$$

and

$$\frac{1}{2}(\mu_A^\alpha + \mu_A^\beta) = G_m^S - x_B^S\frac{\partial G_m^S}{\partial x_B^S} - \eta\frac{\partial G_m^S}{\partial \eta} \quad [11]$$

$$\frac{1}{2}(\mu_B^\alpha + \mu_B^\beta) = G_m^S + (1 - x_B^S)\frac{\partial G_m^S}{\partial x_B^S} - \eta\frac{\partial G_m^S}{\partial \eta}. \quad [12]$$

It can now be seen that Eqn. [2] is equivalent to the ordinary condition for equilibrium order, $\frac{\partial G_m^S}{\partial \eta} = 0$.

3. Thermodynamic Constraint on Solid Composition and Order Parameter During Crystallization

The solidification process must always involve a decrease in free energy ΔG. Baker and Cahn (27) have described the domain of possible solid compositions that can form for various liquid compositions at a given temperature by requiring that $\Delta G \leq 0$ where

$$\Delta G = G_m^S - (\mu_A^L x_A^S + \mu_B^L x_B^S) \quad [13]$$

which is Eqn. [15] of Ref. 27 in a different form. Eqn. [13] is the basis for the usual "tangent to curve rule" to graphically show the change in free energy for a given phase change. Here G_m^S is evaluated for the composition of the solid phase and μ_A^L and μ_B^L are evaluated for the composition of the liquid phase. Application of this principle to the present case will yield domains of possible order parameter and solid composition that can solidify from various liquid compositions at a given temperature. Any prediction of a kinetic model must yield values of η, solid composition, temperature for each liquid composition which will give $\Delta G \leq 0$.

Figure 1 shows schematically the domain of possible order parameter which can form at various temperatures for a congruently melting compound if the liquid composition is equal to the solid composition. These domains as well as the detailed kinetic results described later in this paper depend on whether the ordered phase differs from the disordered phase by a second or first order transition depicted in (a) and (b), respectively. At the top are shown the free energies of the solid and liquid at three temperatures. At the equilibrium melting temperature T_1, only one value of η is possible. Below T_1, $\Delta G \leq 0$ defines a range of possible η given in the cross hatched region in the bottom of the figure. Note that only when the $T \leq T_3$ in (a) or $T \leq T_2$ in (b) can a solid with $\eta = 0$ form. In addition to the range of η which may be possible, a range of ~~liquid~~ composition for each η ~~and solid composition~~ is also described by the condition $\Delta G \leq 0$ (not shown).

4. A Kinetic Model for the Interface

4.1 The Solidification Velocity–Composition Relation

We treat here the case of steady state continuous growth of an atomically rough planar liquid–solid interface. Following the work of Aziz (1) for random crystalline solids, the atomistic interdiffusion flux between adjacent liquid and solid monolayers must have a specific value related to the growth rate and the compositions of the monolayers in order to maintain the steady state. For the growth of an ordered phase, the interdiffusion flux between the liquid and each sublattice must be considered.

To treat interdiffusion between the liquid and solid phase during crystallization we use redistribution potentials $(\mu_B - \mu_A)'$ as defined by Aziz and Kaplan (2)[1]; viz.,

---

[1]Redistribution potentials can also be written in terms of activity coefficients γ_A, γ_B and free energies of the pure components G_A, G_B as $(\mu_B - \mu_A)' = G_B - G_A + RT \ln \gamma_B - RT \ln \gamma_A$.

$$(\mu_B - \mu_A)' = \mu_B - \mu_A - RT\,\ln x_B + RT\,\ln x_A. \qquad [14]$$

Redistribution potentials for the liquid phase, $(\mu_B^L - \mu_A^L)'$, and the α and β sublattices of the solid phase, $(\mu_B^\alpha - \mu_A^\alpha)'$ and $(\mu_B^\beta - \mu_A^\beta)'$ are obtained from a thermodynamic model of the phases.

We consider a pair of reactions from initial states (of B in an α or β site in the solid adjacent to A in the liquid) over a barrier to final states (where the two atoms have exchanged positions) as shown in Figure 2. In a reference frame fixed on the crystal lattice the forward reactions are designated, $J_D^{+\alpha}$ and $J_D^{+\beta}$, and the reverse reactions, $J_D^{-\alpha}$ and $J_D^{-\beta}$, and will be expressed in exchanges per unit time per unit area of α (or β) sublattice. We assume the barrier to redistribution remains a constant height Q_D above the state (initial or final) with the higher redistribution potential. Although other assumptions are possible for the definition of the barrier height this choice is consistent with that used for continuous growth of pure melts (28). Transitions from higher to lower redistribution potential are written as the product of an attempt frequency ν with a Boltzman factor, $\exp\{-\frac{Q_D}{RT}\}$. Transitions from a lower to a higher redistribution potential are written as

$$\nu \exp\{-[Q_D + |(\mu_B^i - \mu_A^i)' - (\mu_B^L - \mu_A^L)'|]/RT\}$$

The state which is higher or lower depends on the values of order parameter and composition.

Due to the above assumptions regarding the barrier heights it is necessary to introduce parameters A_i ($i = \alpha,\beta$) with

$$A_i = \begin{cases} 0 \text{ if } (\mu_B^i - \mu_A^i)' - (\mu_B^L - \mu_A^L)' \geq 0 \\ 1 \text{ if } (\mu_B^i - \mu_A^i)' - (\mu_B^L - \mu_A^L)' < 0\,. \end{cases} \qquad [15]$$

$RT\,\ln \gamma_A$.

Thus the interdiffusion fluxes are given by

$$J_D^{+\alpha} = \frac{f\nu\lambda}{\Omega} x_B^{\alpha}(1 - x_B^L) \exp\left[\frac{-[Q_D + A^{\alpha}|(\mu_B^{\alpha} - \mu_A^{\alpha})' - (\mu_B^L - \mu_A^L)'|]}{RT}\right]$$

$$J_D^{-\alpha} = \frac{f\nu\lambda}{\Omega} x_B^{L}(1 - x_B^{\alpha}) \exp\left[\frac{-[Q_D + (1 - A_{\alpha})|(\mu_B^{\alpha} - \mu_A^{\alpha})' - (\mu_B^L - \mu_A^L)'|]}{RT}\right]$$

$$J_D^{+\beta} = \frac{f\nu\lambda}{\Omega} x_B^{\beta}(1 - x_B^{L}) \exp\left[\frac{-[Q_D + A_{\beta}|(\mu_B^{\beta} - \mu_A^{\beta})' - (\mu_B^L - \mu_A^L)'|]}{RT}\right]$$

$$J_D^{-\beta} = \frac{f\nu\lambda}{\Omega} x_B^{L}(1 - x_B^{\beta}) \exp\left[\frac{-[Q_D + (1 - A_{\beta})|(\mu_B^{\beta} - \mu_A^{\beta})' - (\mu_B^L - \mu_A^L)'|]}{RT}\right]. \quad [16]$$

The parameter f is the fraction of sites at the interface where jumps can occur, λ is the jump distance, and Ω is the atomic volume (assumed the same for A and B). This assumption regarding the barrier heights is identical to that made by Aziz and Kaplan (2). It implies that the exchanges are governed by the properties of the interface and not the bulk solid or liquid phases. One also could have introduced separate Q_D^{α} and Q_D^{β} for the exchanges from the two sublattices, the consequences of which will be deferred to the discussion section of this paper.

The net diffusive fluxes, J_D^{α}, and J_D^{β}, are then

$$J_D^{\alpha} = J_D^{+\alpha} - J_D^{-\alpha}$$

$$= D_i/(\lambda\Omega)[x_B^{\alpha}(1 - x_B^L)K_{\alpha}^{A_{\alpha}} - x_B^L(1 - x_B^{\alpha})K_{\alpha}^{(1 - A_{\alpha})}] \quad [17]$$

and $J_D^{\beta} = J_D^{+\beta} - J_D^{-\beta}$

$$= D_i/(\lambda\Omega)[x_B^{\beta}(1 - x_B^L)K_{\beta}^{A_{\beta}} - x_B^L(1 - x_B^{\beta})K_{\beta}^{(1 - A_{\beta})}] \quad [18]$$

where

$$K_{\alpha} = \exp\left[\frac{-|(\mu_B^{\alpha} - \mu_A^{\alpha})' - (\mu_B^{L} - \mu_A^{L})'|}{RT}\right]$$
$$K_{\beta} = \exp\left[\frac{-|(\mu_B^{\beta} - \mu_A^{\beta})' - (\mu_B^{L} - \mu_A^{L})'|}{RT}\right] \qquad [19]$$

and

$$D_i = f\nu\lambda^2 \exp\{-\frac{Q_D}{RT}\} \qquad [20]$$

which is called the interface diffusivity.

In order to maintain steady state conditions at the growing interface a mass balance must be satisfied. In order to extract a simple model for the present we will assume that interdiffusion in the liquid is fast enough to prevent lateral composition variations in the first liquid monolayer and that interdiffusion in the solid is slow enough that lateral exchanges (ordering) in the first solid monolayer do not occur. In this case mass balance requires that

$$J_D^{\alpha} = \frac{V}{\Omega}(x_B^{L} - x_B^{\alpha})$$
$$J_D^{\beta} = \frac{V}{\Omega}(x_B^{L} - x_B^{\beta}) \qquad [21]$$

where V is the interface velocity. Equating expressions for the net diffusive fluxes we obtain

$$x_B^{\alpha}(1 - x_B^{L})K_{\alpha}^{A_{\alpha}} - x_B^{L}(1 - x_B^{\alpha})K_{\alpha}^{(1 - A_{\alpha})} = \frac{V}{V_D}(x_B^{L} - x_B^{\alpha})$$
$$x_B^{\beta}(1 - x_B^{L})K_{\beta}^{A_{\beta}} - x_B^{L}(1 - x_B^{\beta})K_{\beta}^{(1 - A_{\beta})} = \frac{V}{V_D}(x_B^{L} - x_B^{\beta}) \qquad [22]$$

where $V_D = D_i/\lambda$.

One may choose to solve these equations for a given V and x_B^{L} in order to find the compositions of the α and β sublattices. This would yield the average solid composition and the long range order parameter at the interface. For this purpose we require the

redistribution potentials which depend on temperature and the various compositions through a specific thermodynamic model of the liquid and solid phases. To determine the temperature of the interface an additional equation relating the solidification velocity to the driving force for solidification is required.

4.2 The Solidification Velocity–Temperature Relation

We will assume (28) that the solidification velocity V is related to the free energy change for crystallization of ΔG according to

$$V = V_C \left[1 - \exp\left(\frac{\Delta G}{RT}\right)\right] \qquad [23]$$

where V_C is a crystallization rate parameter. Following the general concept that crystallization is easier than solute redistribution, V_C is assumed greater than V_D. In the case of collision limited growth, V_C may approach the speed of sound. If diffusive jumps are required for crystallization V_C can be approximated by the ratio of the liquid diffusion coefficient to λ, the jump distance. Thus, given thermodynamic potentials for the phases and kinetic parameters V_D and V_C, Eqns. [22] and [23] give the order parameter, liquid composition, and temperature at the interface for any solid composition and solidification velocity.

5. Choice of Thermodynamic Potentials

The predictions of this model will be examined for phase diagrams having a congruently melting ordered phase at $x_B^S = \frac{1}{2}$. Thus the order–disorder temperature of the solid phase must be chosen to be higher than the congruent melting temperature. The following form of the solid free energy, G_m^S, will also permit the comparison of the predictions when this order–disorder transition is first–order and second–order:

$$\begin{aligned} G_m^S = {} & G_A^S(1 - x_B^S) + G_B^S x_B^S \\ & + \Omega_1\left\{x_B^S(1 - x_B^S) + \tfrac{1}{4}\eta^2\right\} \\ & + \Omega_2\eta^4 \end{aligned} \qquad [24]$$

$$+ \tfrac{1}{2}\,RT\left\{(x_B^S - \tfrac{1}{2}\eta)\,\ell n\,(x_B^S - \tfrac{1}{2}\eta) + (x_B^S + \tfrac{1}{2}\eta)\,\ell n\,(x_B^S + \tfrac{1}{2}\eta)\right.$$
$$\left. + (1 - x_B^S - \tfrac{1}{2}\eta)\,\ell n\,(1 - x_B^S - \tfrac{1}{2}\eta) + (1 - x_B^S + \tfrac{1}{2}\eta)\,\ell n\,(1 - x_B^S + \tfrac{1}{2}\eta)\right\}$$

where G_A^S and G_B^S are the free energies of pure solid A and B and Ω_1 and Ω_2 are constants. If $\Omega_2 = 0$ and $\Omega_1 < 0$, Eqn. [24] describes a Bragg–Williams phase with near neighbor interaction Ω_1 and ideal entropy. The η–dependence of the free energy curve for $x_B^S = \frac{1}{2}$ is shown schematically in Figure 1a. The transition between the ordered and disordered phase is a second order phase transition; i.e., the equilibrium order parameter goes to zero continuously as temperature is increased. If $\Omega_2 < 0$ and $\Omega_1 > 12\Omega_2$ the ~~free~~ η–dependence of the free energy curve for $x_B^S = \frac{1}{2}$ is shown schematically in Figure 1b. The transition between ordered and disordered phase is a first order phase transformation; i.e., the equilibrium order parameter has a discontinuous drop to zero.

For the choice of G_m^S given in Eqn. [24], Eqns. [9–12] give

$$\mu_B^\alpha - \mu_A^\alpha = G_B^S - G_A^S + \Omega_1(1 - 2x_B^S - \eta) - 8\Omega_2\eta^3$$
$$+ RT\,\{\ell n\,(x_B^S - \tfrac{1}{2}\eta) - \ell n\,(1 - x_B^S + \tfrac{1}{2}\eta)\}$$
$$\mu_B^\beta - \mu_A^\beta = G_B^S - G_A^S + \Omega_1(1 - 2x_B^S + \eta) + 8\Omega_2\eta^3$$
$$+ RT\,\{\ell n\,(x_B^S + \tfrac{1}{2}\eta) - \ell n\,(1 - x_B^S - \tfrac{1}{2}\eta)\}, \qquad [25]$$

$$\tfrac{1}{2}(\mu_A^\alpha + \mu_A^\beta) = G_A^S + \Omega_1\{(x_B^S)^2 - \tfrac{1}{4}\eta^2\} - 3\Omega_2\eta^4$$
$$+ \tfrac{1}{2}\,RT\,\{\ell n\,[(1 - x_B^S)^2 - \tfrac{1}{4}\eta^2]\}$$
$$\tfrac{1}{2}(\mu_B^\alpha + \mu_B^\beta) = G_B^S + \Omega_1\{(1 - x_B^S)^2 - \tfrac{1}{4}\eta^2\} - 3\Omega_2\eta^4$$
$$+ \tfrac{1}{2}\,RT\,\{\ell n\,[(x_B^S)^2 - \tfrac{1}{4}\eta^2]\} \qquad [26]$$

and

$$(\mu_B^\alpha - \mu_A^\alpha)' = G_B^S - G_A^S + \Omega_1(1 - 2x_B^S - \eta) - 8\Omega_2\eta^3$$
$$(\mu_B^\beta - \mu_B^\beta)' = G_B^S - G_A^S + \Omega_1(1 - 2x_B^S + \eta) + 8\Omega_2\eta^3. \qquad [27]$$

For the liquid phase we will employ a regular solution model with

$$\mu_A^L = G_A^L + \Omega^L (x_B^L)^2 + RT\, \ell n\, (1 - x_B^L)$$
$$\mu_B^L = G_B^L + \Omega^L (1 - x_B^L)^2 + RT\, \ell n\, x_B^L \qquad [28]$$

where G_A^L and G_B^L are free energies of pure liquid A and B. The redistribution potential is given by

$$(\mu_B^L - \mu_A^L)' = G_B^L - G_A^L + \Omega^L (1 - 2x_B^L). \qquad [29]$$

Further we will assume that

$$G_A^L - G_A^S = G_B^L - G_B^S = S(T_m - T) \qquad [30]$$

where S and T_m are the entropy of fusion and melting point of the pure components (assumed equal). Eqn. [30] will guarantee a phase diagram which is symmetric about $x_B = \frac{1}{2}$.

6. Approximate Result for Dependence of Order Parameter on Velocity at a Congruent Melting Maximum

A simple expression can be obtained from Eqns. [22] for $x_B^L = \frac{1}{2}$ which will provide some insight into the numerical results described in Section 7. Both equations are satisfied if $x_B^S = \frac{1}{2}$ and if the order parameter satisfies

$$\frac{\Omega_1 \eta + 8\Omega_2 \eta^3}{RT} = \ell n \left[\frac{(1 - \eta) - 2\frac{V}{V_D}\eta}{1 + \eta} \right] \qquad [31]$$

for $\eta \geq 0$[2]. Note that two solutions, $\eta = 0$ and $\eta \neq 0$, exist. For $V = 0$ this equation gives the equilibrium order parameter as a function of T for $x_B^S = 0.5$ which could also have been found using Eqn. [2]. As a kinetic equation for solidification, T represents the interface temperature which can only be determined using Eqn. [23] in combination with Eqn. [31]. However, if we consider that the interface temperature may be approximated

---

[2]For $\eta \geq 0$, Eqn. [31] is modified due to the A_i factors and the theory predicts the same behavior for $\pm \eta$.

by the melting point of the ordered phase T_m^o, then Eqn. [31], after rearrangement, becomes

$$\frac{V}{V_D} \cong \frac{1}{2\eta}\left\{(1-\eta) - (1+\eta)\exp\left[\frac{\Omega_1\eta + 8\Omega_2\eta^3}{RT_m^o}\right]\right\}. \qquad [32]$$

This approximation predicts that η goes to zero as $\frac{V}{V_D}$ goes to $(-\frac{\Omega_1}{2RT_m^o} - 1)$. For the case where $\Omega_2 = 0$, the critical temperature for the order–disorder transition T_c is equal to $(-\frac{\Omega_1}{2R})$. Therefore the critical value of $\frac{V}{V_D}$ where the long range order parameter goes to zero is given by

$$(\frac{V}{V_D})_{\eta = 0} \approx \frac{T_c}{T_m^o} - 1 \qquad [34]$$

and hence the critical velocity is high when T_c is high (i.e., when the ordering is strong). When $\Omega_2 \neq 0$, the critical velocity follows the same trend but is not so simply estimated.

7. Numerical Results

We will examine in parallel the calculated phase diagram and results of the non–equilibrium interface theory for two cases with thermodynamic parameters given in Table I.

Table I. Choice of Thermodynamic Parameters

	T_m(K)	S/R	Ω_L/R(K)	Ω_1/R(K)	Ω_2/R(K)
Case I	1000K	2	0	–3000	0
Case II	1000K	2	0	–2000	–566.2

7.1 Equilibrium Phase Diagram

Figures 3a and 3b show the equilibrium order parameter, η_e, of the solid as a

function of T for the two cases for $x_B^S = 0.5$, obtained using Eqn. [2]. In I, the order–disorder (OD) temperature is 1500 K ($-\frac{\Omega_1}{2R}$). In II, the OD temperature is 1583 K and is obtained by finding the temperature where G_S for $\eta = 0$ is equal to G_S for $\eta = \eta_e$. The dashed curve represents states where the ordered phase is metastable whereas the dotted curve represents states where the ordered phase is unstable. Cases I and II are respectively second and first order transitions.

Figures 4a and 4b show half of the phase diagrams for the solid phases only. In Figure 4a no two–phase field exists between the ordered and disordered phase, characteristic of the second order transition. The curve is obtained from Eqn. [2] by letting $\eta \to 0$. In Figure 4b a two–phase field exists. The boundaries are obtained by equating the values of $\frac{1}{2}(\mu_A^\alpha + \mu_A^\beta)$ for $\eta = 0$ and $\eta = \eta_e$ obtained from Eqn. [2] and similarly the values of $\frac{1}{2}(\mu_B^\alpha + \mu_B^\beta)$.

Figures 5a and 5b show the equilibrium diagrams using Eqns. [3] in combination with Eqn. [2] to generate the liquid–solid equilibrium. In both cases the melting point of the composition $x_D = 0.5$ is below the OD temperature. The diagrams contain "peritectic reactions," L + O → D; however, in Figure 5a no discontinuity in slope occurs at the liquidus at the "peritectic temperature" due to the second order nature of the OD reaction. For case II a metastable liquidus and solidus are shown dashed for the disordered phase. For case I such curves would represent unstable equilibrium and are not shown.

7.2 Non–Equilibrium Interface Conditions for Congruently Melting Ordered Phase

In general there are two solutions to Eqns. [22] and [23] for the non–equilibrium interface conditions: one for $\eta = 0$ and one for $\eta \neq 0$. The $\eta \neq 0$ solution only exists below some critical value of V/V_D. Different parts of each solution are stable or unstable in the sense that small fluctuations in the order parameter will lead to large changes in the

interface conditions. Unstable portions will be shown dotted in the following figures. The details of this stability analysis will be deferred until the discussion.

For $x_B^S = 0.5$ Eqns. [22] and [23] are satisfied for $x_B^L = 0.5$ and values of η and T as a function of $\frac{V}{V_D}$ shown in Figures 6 and 7. For these results $\frac{V_C}{V_D}$ was chosen to be 10^3. In Figure 6a for case I, the order parameter goes to zero continuously as a critical value of $\frac{V}{V_D}$ is reached. In Figure 6b for case II the order parameter exhibits a turning or limit point at a critical value of $\frac{V}{V_D}$. If the velocity is increased above the limit point, the order parameter must jump discontinuously to the $\eta = 0$ solution in case II. In Figure 6b the branch below the turning point is dotted and represents unstable solutions. At $V = 0$ this unstable branch corresponds to the thermodynamically unstable equilibrium between the liquid and solid (see $T = T_3$ in Figure 1b).

In Figure 7, the interface temperatures for the $\eta = 0$, and $\eta \neq 0$ solutions are shown. Again the dotted portions are unstable. For case I, the $\eta = 0$ solution is only stable above the critical velocity. For case II the $\eta = 0$ solution is always stable and corresponds to the solidification of the metastable disordered phase.

Figure 8 shows cross plots of η and T. Points along these curves are parameterized by $\frac{V}{V_D}$. Also included in the figure are the equilibrium order parameter, η_e, versus temperature as shown originally in Figure 3.

7.3 Simultaneous Disorder and Solute Trapping

For compositions away from the congruent maximum of the ordered phase, the possibility of non–equilibrium incorporation of solute (solute trapping) as well as disorder trapping is possible. Figures 9 and 10 show the order parameter and liquid composition at the interface as a function of V/V_D for $x_B^S = 0.48$ for the two cases. The behavior of the order parameter is quite similar to that for $x_B^S = 0.5$. Figure 10 is shown with a

logarithmic scale for velocity to permit comparison to previous theory (1–2) on solute trapping of disordered solids. In both cases I and II the composition of the liquid approaches the composition of the solid at high velocity.

Near the velocity where η goes to zero in case I or where the turning point occurs in case II in Figure 9, the liquid compositions shown in Figure 10 have abrupt changes. In case I the lower curve for the $\eta \neq 0$ solution merges with that for the $\eta = 0$ solution. Below this merge point the $\eta = 0$ solution is unstable and is shown dotted. In case II, the liquid composition curve for the $\eta = 0$ solution is stable for all velocities. The liquid composition for the $\eta \neq 0$ solution exhibits a turning point at the same velocity where η has a turning point in Figure 9b. In this case the lower branch is stable and the upper branch is unstable. Thus for case II the theory predicts that with increasing velocity a jump in liquid composition at the interface occurs when η goes to zero. As shown, the size of the jump is small but it of course depends on the thermodynamic potentials used.

It is also interesting to note that in case I η goes to zero at velocities where solute redistribution remains significant while in case II complete disorder trapping occurs at a velocity where solute trapping is practically complete. Numerical results for other values of Ω_1 and Ω_2 not described here suggest that this is not a general trend for solid phases with first and second order transitions.

8. Discussion

The validity of the assumptions regarding complete mixing in the first liquid monolayer and the absence of lateral atomic rearrangements in the first solid monolayer are ultimately tied to the values of the interdiffusion coefficients in the solid (D_S), interface (D_i), and liquid (D_L). In general it is reasonable to assume that $D_S < D_i < D_L$. The present theory best applies when these differ by orders of magnitude. However, even if D_i approaches D_L, the assumption of complete mixing in the first liquid monolayer may

only become suspect if the atom positions of each sublattice stays fixed laterally on the liquid solid interface during growth. This could happen in some crystallographic orientations of some crystal structures; e.g., growth of a chemically layered structure edgewise into the melt. In this case one would expect disorder trapping at lower solidification rates than predicted by this theory. Relaxation of the assumption regarding no ordering in the first solid monolayer would increase the state of order at any velocity over that predicted by the theory. This ordering of the surface layer could be added to that which occurs during solid state cooling to predict the state of order in a final (cold) solid. The theory also has assumed that $Q_D^{\alpha} = Q_D^{\beta}$ or that the interdiffusion between the liquid and solid do not depend on the sublattice. This condition can easily be relaxed. One result of such a change would be that for solidification of a composition at a congruent melting maximum, x_B^L would not equal x_B^S except at $V = 0$ and $V = \infty$.

The results of the dependence of η on $\frac{V}{V_D}$ may be viewed in the context of bifurcation theory. Bifurcation theory describes the change in stability of solutions near intersection (bifurcation) points and turning points. The two solutions $\eta = 0$ and $\eta \neq 0$ always intersect at $\frac{V}{V_D} \approx -\frac{\Omega_1}{2RT_m^o} - 1$, which occurs at positive and negative values of $\frac{V}{V_D}$, for case I and II respectively. At this point the stability of the $\eta = 0$ solution must change. By replacing Eqn. [31], which applies only for the steady state, with the time dependent form of the flux balance, one obtains for $x_B = 0.5$

$$\frac{d\eta}{dt} = -\frac{1}{2}\left\{2\frac{V}{V_D}\eta - (1-\eta) + (1+\eta)\exp\left[\frac{\Omega_1\eta + 8\Omega_2\eta^3}{RT_m^0}\right]\right\} \qquad [35]$$

for $\eta \geq 0$,

from which the stability of the various solutions can be inspected. If a positive perturbation of η makes the RHS of Eqn. [35] positive then $\frac{d\eta}{dt} < 0$ and the perturbation decays and that

portion of the solution is stable. Using this method the $\eta = 0$ solution can be shown to be stable only if $\frac{V}{V_D} > -1 - \frac{\Omega_1}{2RT_m^o}$. Similarly the stability of the $\eta \neq 0$ solutions can be inspected. In case I, the $\eta \neq 0$ solution is always stable while the $\eta \neq 0$ solution for case II must change from stable to unstable at the turning point. The stable branch has negative slope in the η versus $\frac{V}{V_D}$ plot.

The slope of the curves in Figure 7, $\frac{dT}{dV}$ are worthy of some discussion. The slope is called the interface kinetic coefficient μ and relates a simple measure of the departure from equilibrium required to cause growth at various rates. It can be seen that the slope is small near $V = 0$ and whenever $\eta = 0$. At velocities where η is changing, the slope is much steeper; i.e., the kinetics become more "sluggish." A complex expression for $\frac{dT}{dV}$ can be found for $x_B = \frac{1}{2}$ by differentiation of Eq. [23] and [24].

Near $V = 0$ or when $\eta = 0$, the kinetic coefficient is $-\frac{RT_m^o}{\Delta S}(\frac{1}{V_C})$ where ΔS is the applicable entropy of fusion. When η is changed rapidly the kinetic coefficient depends on ~~both~~ V_C also ~~and~~ V_D. Thus the growth kinetics are controlled by V_C either when the solid is disordered or when the solid is ordered at small V. At intermediate V the kinetics are controlled by a combination of V_C and V_D when the solid is ordered.

The present theory can provide some guidance in selecting intermetallic compounds which respond to rapid solidification to produce phases with non-equilibrium composition or state of order. The former may be useful to provide the supersaturation necessary to form a controlled scale of precipitation by subsequent heat treatment. Non-equilibrium order produced by solidification will often be followed by rapid ordering during solid state cooling. The fine antiphase domains structures produced by this process can provide unusual starting materials for subsequent heat treatment (30).

It is important to note that many complex ordered phases such as σ phases bear no resemblance to simple disordered structures. The elimination of such phases by rapid solidification and replacement by a simpler disordered phase is not an example where this theory is applicable. Classical concepts of nucleation and growth competition must be applied to these situations.

Quantitative predictions by this theory require good thermodynamic models for the phases of interest as well as values for the kinetic parameters V_C and V_D. Unfortunately, measurements of equilibrium order parameter are often not available, especially for materials of technological interest with high melting points. Thus the data base for thermodynamic modelling is poor. Additionally functional forms of the thermodynamic potentials used for ordered phase in many phase diagram evaluations have improper functional form near $\eta = 0$. This will severely impact the predictions of this theory. Values of V_C and V_D can only be crudely estimated. Experiments on combined solute trapping and disorder trapping using pulsed laser annealing with the transient conductance method to measure interface rates may provide insight in these parameters. An analysis of the rate of ordering during solid state cooling must be included to obtain the values produced by the interface itself. Two features are amenable to measurement. Extremely fine antiphase domains should be present if the critical velocity has been exceeded. Also the abrupt behavior of the composition shown in Figure 10 when η goes to zero may produce unusual microstructural features.

Acknowledgement

The authors would like to thank J. W. Cahn for assistance in dealing with the thermodynamics of ordered phases. Discussions with S. R. Coriell are greatly appreciated. This research was supported by DARPA (Order #6065) for W.J.B. and by the National Science Foundation for M.J.A.

References

1. M. J. Aziz, J. Appl. Phys. 53, 1158 (1982).

2. M. J. Aziz and T. Kaplan, Acta Metall. 36, 2335 (1988).

3. L. M. Goldman and M. J. Aziz, J. Mater. Res. 2, 524 (1987).

4. K. A. Jackson, in Surface Modification and Alloying by Laser, Ion and Electron Beams, eds. J. M. Poate, G. Foti and D. C. Jacobson (Plenum, New York, 1983), p. 62; G. H. Gilmer, Mat. Res. Soc. Symp. Proc. 13, 249 (1983)

5. G. H. Gilmer, Mat. Res. Soc. Symp. Proc. 13, 249 (1983).

6. J. W. Cahn, S. R. Coriell and W. J. Boettinger, in Laser and Electron Beam Processing of Materials, eds. C. W. White and P. S. Peercy (New York, Academic, 1980), p. 89.

7. V. V. Voronkov and A. A. Chernov, Sov. Phys. Cryst. 12, 186 (1967).

8. H. Pfeiffer, Phys. Stat. Solidi (a) 99, 139 (1980).

9. D. E. Temkin, Sov. Phys. – Crystallogr. 17, 405 (1972).

10. M. J. Aziz, J. Y. Tsao, M. O. Thompson, P. S. Peercy and C. W. White, Phys. Rev. Lett. 56, 2489 (1986).

11. M. J. Aziz and C. W. White, Phys. Rev. Lett. 57, 2675 (1986).

12. C. C. Koch, J. A. Horton, C. T. Liu, O. B. Cavin, and J. O. Scarbrough, in Rapid Solidification Processing: Principles and Technologies, Vol. 3, ed. R. Mehrabian,National Bureau of Standards, Washington, DC, 1982, p. 264.

13. A. Inoue, T. Masumoto, H. Tomioka, and N. Yano, Int. J. Rapid Solidification 1, 115 (1984).

14. S. C. Huang, E. L. Hall, K. M. Chang, and R. P. Laforce, Metall. Trans. A 17, 1685 (1986).

15. W. J. Boettinger, L. A. Bendersky, F. S. Biancaniello and J. W. Cahn, Mat. Sci. Eng.

98, 273 (1988).

16. T. Meister and H. Muller–Krumbhaar, Phys. Rev. Lett. 51, 1789 (1983).

17. P. R. Harrowell and D. W. Oxtoby, J. Chem. Phys. 86, 2932 (1987).

18. A. A. Chernov, Sov. Phys. Uspekhi 13, 101 (1970).

19. E. A. Brenner and D. E. Temkin, Sov. Phys. Crystallogr. 28, 7 (1983).

20. T. A. Cherapanova, A. V. Shirin, and V. T. Borisov, Sov. Phys. Crystallogr. 22, 147 (1977).

21. P. Bennema and J. P. Van der Eerden, J. Cryst. Growth 42, 201 (1977).

22. T. Chevapanova, J. P. Van der Eerden, and P. Bennema, J. Cryst. Growth 44 537 (1978).

23. S. R. Coriell and D. Turnbull, Acta Metall. 30, 2135 (1982).

24. C. A. MacDonald, A. M. Malvezzi and F. Spaepen, Mat. Res. Soc. Symp. Proc. 51, 277 (1986).

25. J. Q. Broughton, G. H. Gilmer, and K. A. Jackson, Phys. Rev. Lett. 49, 1496 (1982).

26. T. Kaplan, M. J. Aziz and L. J. Gray, submitted to J. Chem. Phys.

27. J. C. Baker and J. W. Cahn, in Solidification, ASM (1971), 23.

28. D. Turnbull, J. Phys. Chem. 66, 609 (1962).

29. see for example, G. Iooss and D. D. Joseph, Elementary Stability and Bifurcation Theory, Springer–Verlag, New York, NY, 1980.

30. L. A. Bendersky, P. W. Voorhees, W. J. Boettinger, and W. C. Johnson, Scripta met. 22, 1029 (1988).

Figure Captions

Figure 1. Schematic representation of the origin of the thermodynamic constraint on η during non–equilibrium solidification of a congruently melting ordered phase. The ordered solid phase may differ from the disordered solid phase by (a) a second order transition ~~and~~ or (b) a first order phase transition. Top, solid free energy versus η and liquid free energy varies temperatures T_1, T_2, T_3. T_1 is the equilibrium melting point of the ordered phase, T_2 is an arbitrary temperature for (a) and the metastable melting point of the disordered phase for (b), and T_3 is the unstable melting point of the ordered phase. The condition, $G_S - G_L < 0$, defines a range of η as a function of solidification temperature where solidification is possible at the bottom.

Figure 2. Reaction coordinate diagram for interface redistribution reaction. Initial states: B on α or β site in solid, A in liquid. Final states: A on α or β site in solid, B in liquid.

Figure 3. Calculated equilibrium long range order parameter in the solid, η, as a function of temperature for $x_B^S = 0.5$ (a) Case I, order–disorder temperature is 1500 K. (b) Case II, order–disorder temperature is 1583 K, dashed curve – metastable ordered state, dotted curve unstable ordered state.

Figure 4. Calculated phase diagram for solid phase only for (a) Case I and (b) Case II. (Diagram is symmetric about $x_B = 0.5$).

Figure 5. Calculated equilibrium phase diagram for (a) Case I and (b) Case II. In (b) the dashed curve corresponds to the metastable liquidus and solidus for the disordered phase.

Figure 6. Long range order parameter of the solid at the interface, η, as a function of dimensionless growth velocity, V/V_D for the congruently melting compound at $x_B^S = 0.5$. (a) Case I, (b) Case II. Capital letters designate the common interface conditions in Figures 6, 7, and 8.

Figure 7. Interface temperature T as a function of dimensionless growth velocity, $\frac{V}{V_D}$ for

the congruently melting compound at $x_B^S = 0.5$. (a) Case I, (b) Case II. The dashed curves correspond to the $\eta = 0$ solution.

Figure 8. Cross plot of order parameter and interface temperature parameterized by $\frac{V}{V_D}$ for (a) Case I and (b) Case II. Also shown are the equilibrium order parameter at the various temperatures taken from Figure 3.

Figure 9. Long range order parameter of the solid at the interface, η, as a function of dimensionless growth velocity, V/V_D for (a) Case I with $x_B^S = .48$, and (b) Case II with $x_B^S = 0.48$. Capital letters designate common interface conditions in Figures 9 and 10.

Figure 10. Liquid composition at the interface x_B^L, as a function of dimensionless growth velocity V/V_D same cases as Figure 9.

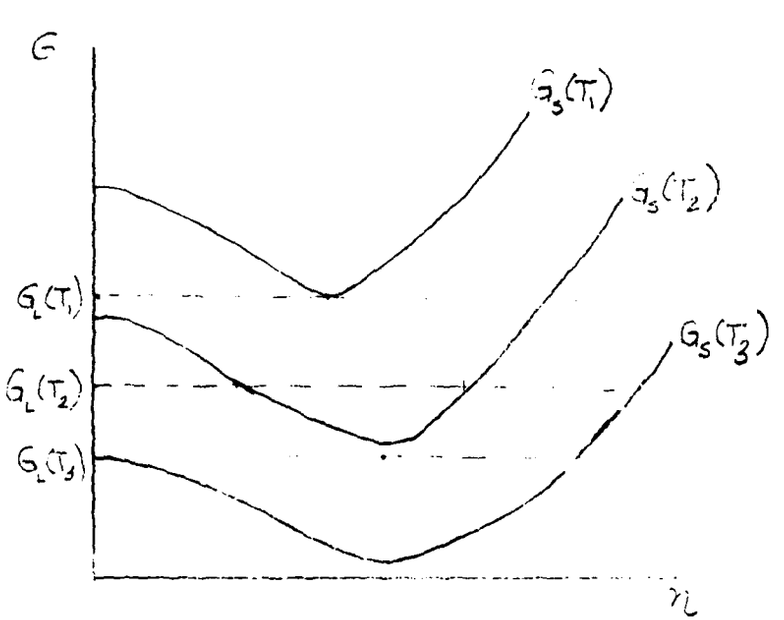
G
$G_s(T_1)$
$G_s(T_2)$
$G_s(T_3)$
$G_L(T_1)$
$G_L(T_2)$
$G_L(T_3)$
η

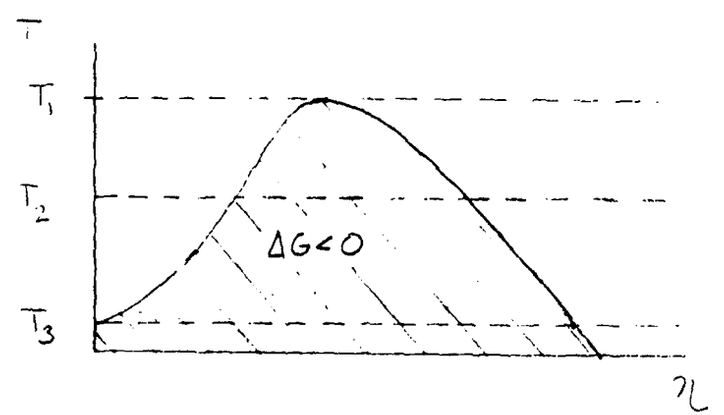
T
T_1
T_2
T_3
ΔG<0
η

(a)

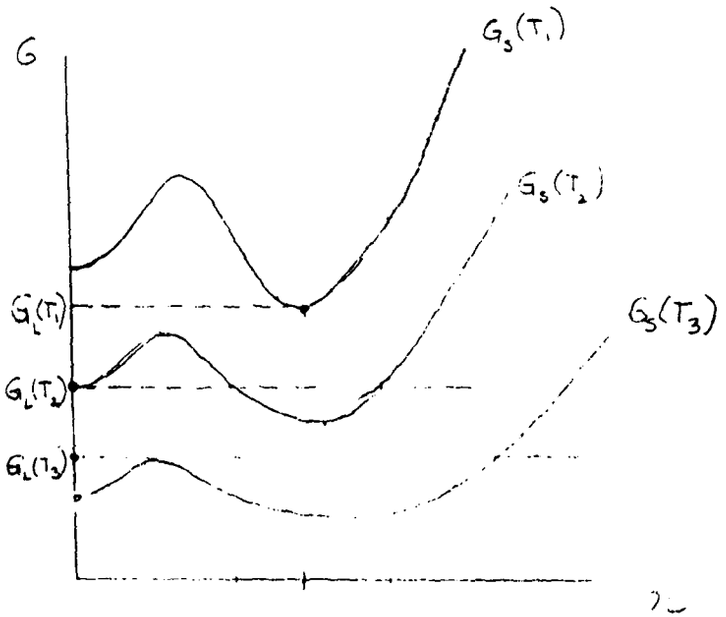
G
$G_s(T_1)$
$G_s(T_2)$
$G_s(T_3)$
$G_L(T_1)$
$G_L(T_2)$
$G_L(T_3)$
η

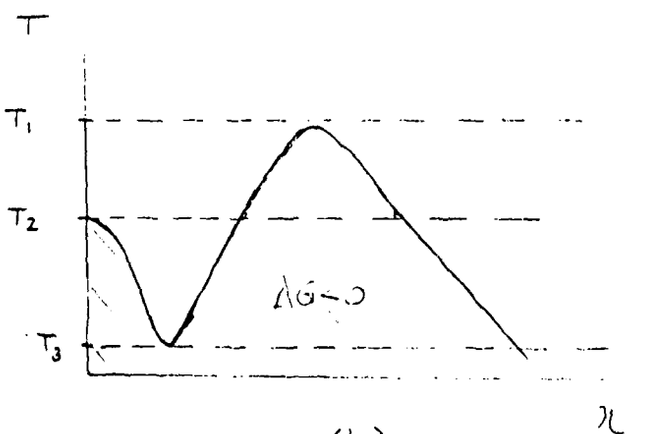
T
T_1
T_2
T_3
ΔG<0
η

(b)

FIG 1

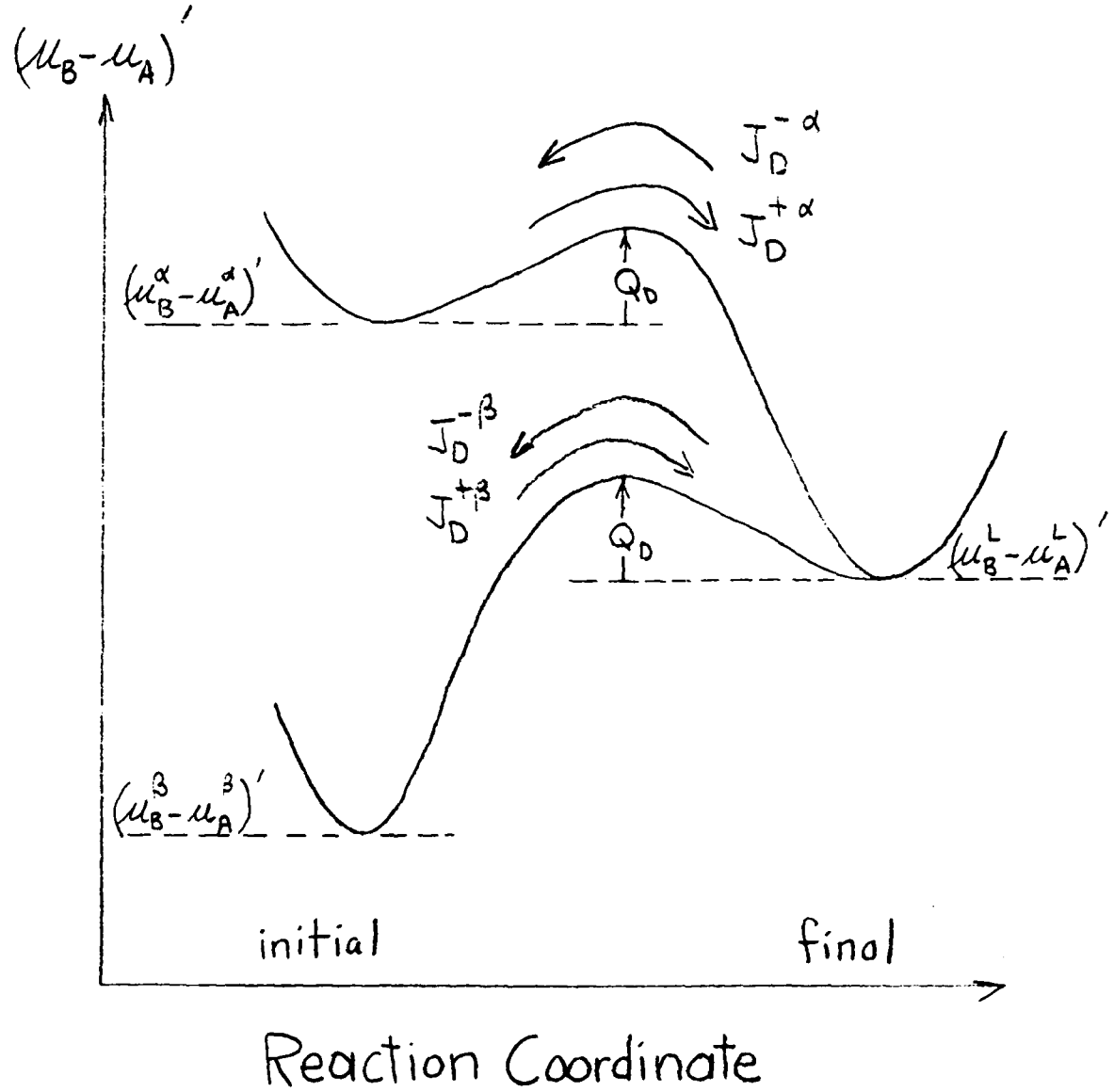
$(\mu_B - \mu_A)'$
$J_D^{-\alpha}$
$J_D^{+\alpha}$
$(\mu_B^\alpha - \mu_A^\alpha)'$
Q_D
$J_D^{-\beta}$
$J_D^{+\beta}$
Q_D
$(\mu_B^L - \mu_A^L)'$
$(\mu_B^\beta - \mu_A^\beta)'$
initial
final
Reaction Coordinate

FIG 2

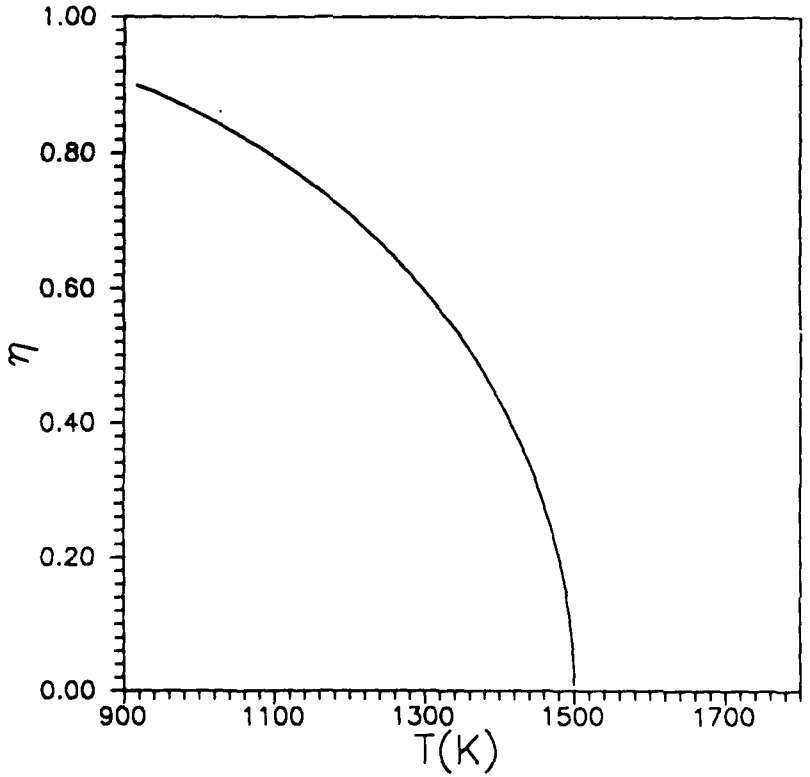
1.00
0.80
0.60
0.40
0.20
0.00
η
900
1100
1300
1500
1700
T(K)

(a)

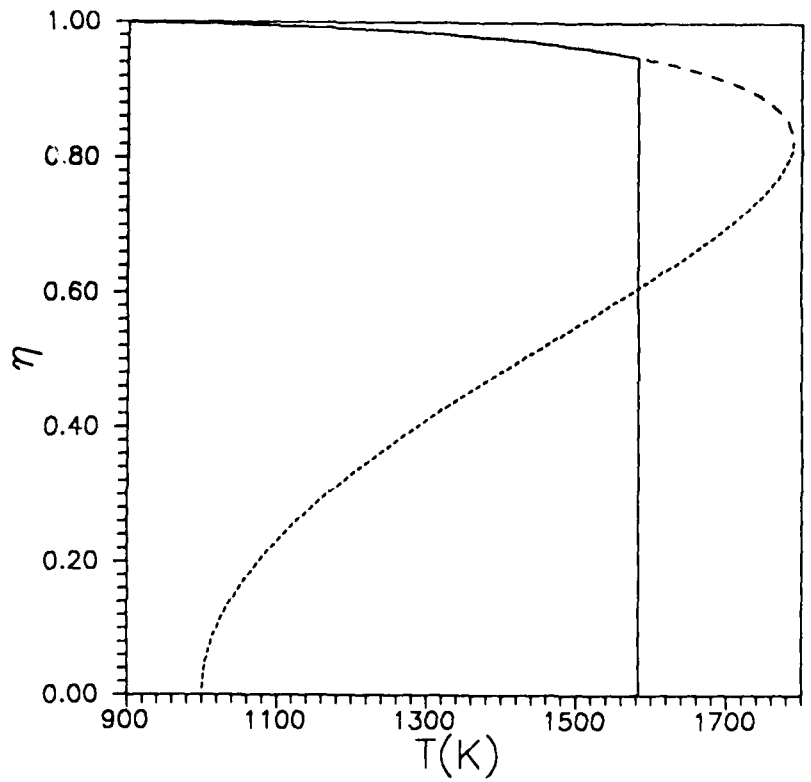
1.00
0.80
0.60
0.40
0.20
0.00
η
900
1100
1300
1500
1700
T(K)

(b)

FIG 3

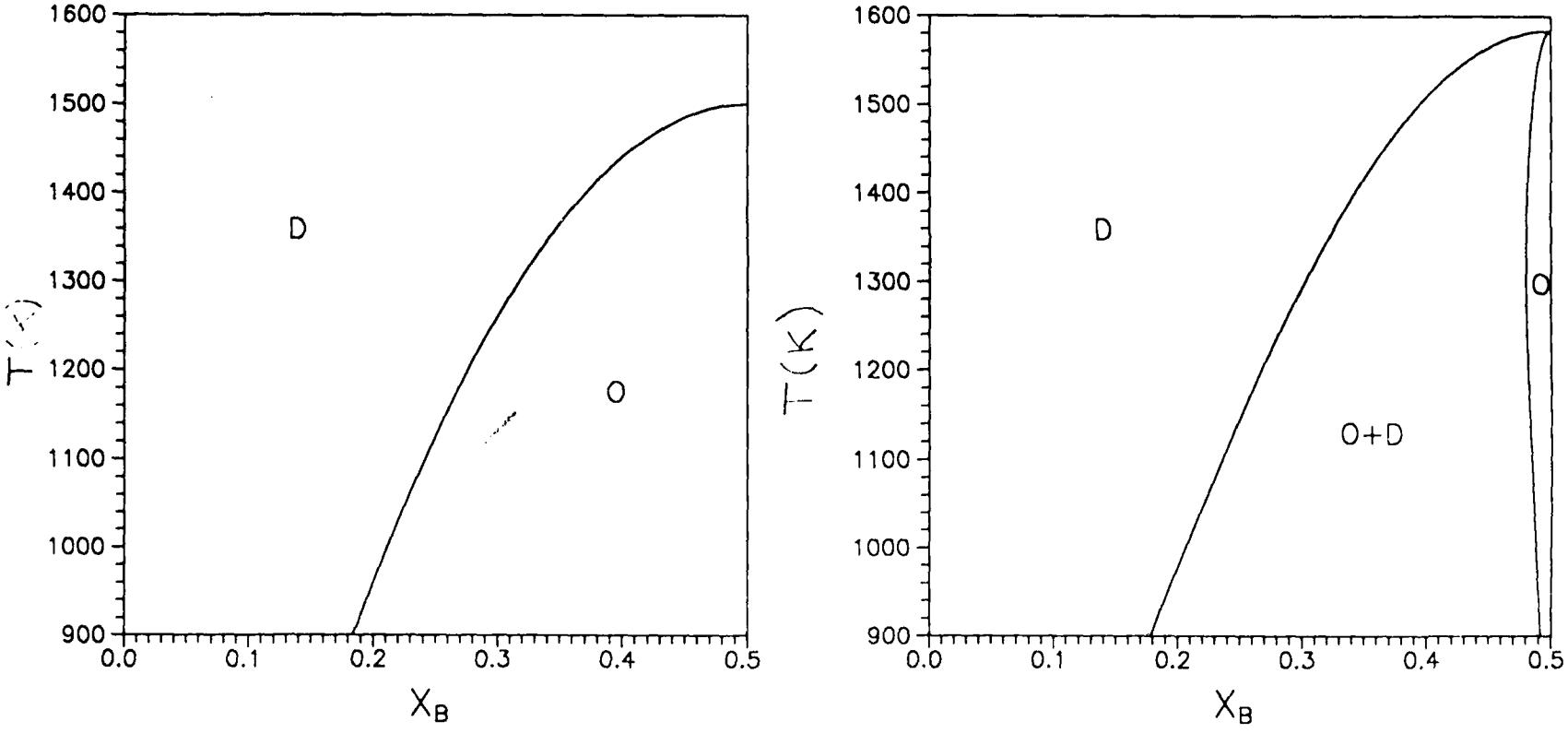
1600
1500
1400
1300
1200
1100
1000
900
T(K)
D
O
0.0
0.1
0.2
0.3
0.4
0.5
X_B
(a)
1600
1500
1400
1300
1200
1100
1000
900
T(K)
D
O
O+D
0.0
0.1
0.2
0.3
0.4
0.5
X_B
(b)

Fig 4

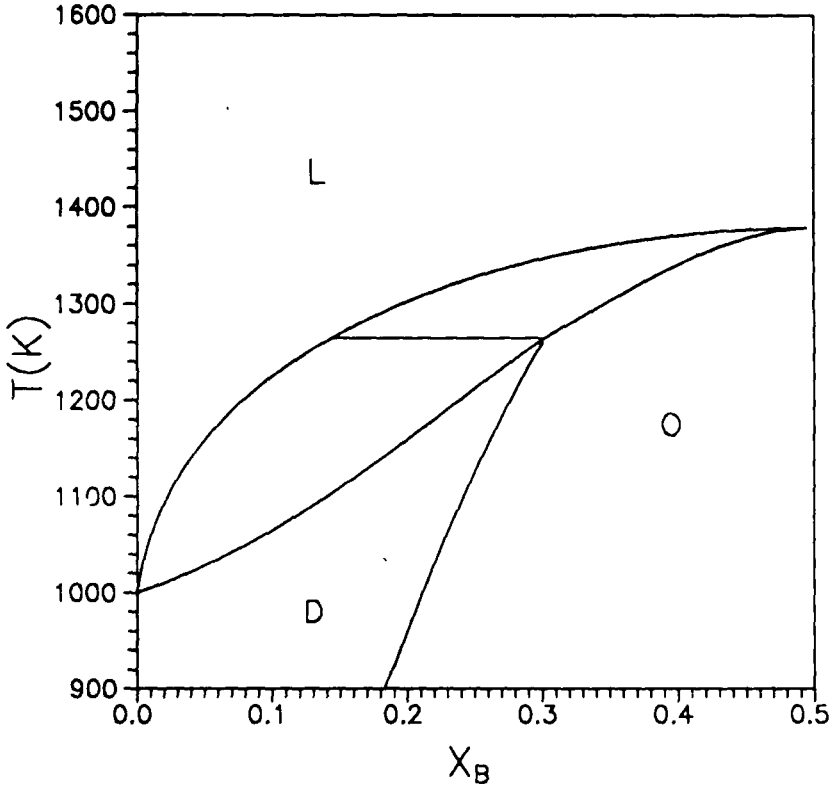
1600
1500
1400
1300
1200
1100
1000
900
T(K)
L
O
D
0.0
0.1
0.2
0.3
0.4
0.5
X_B

(a)

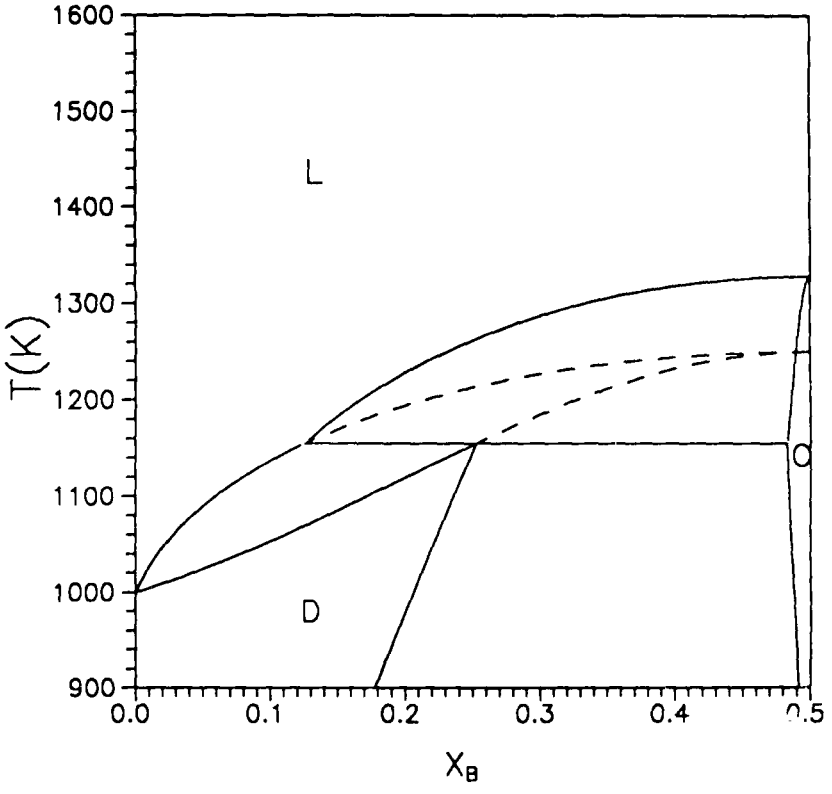
1600
1500
1400
1300
1200
1100
1000
900
T(K)
L
O
D
0.0
0.1
0.2
0.3
0.4
0.5
X_B

(b)

FIG 5

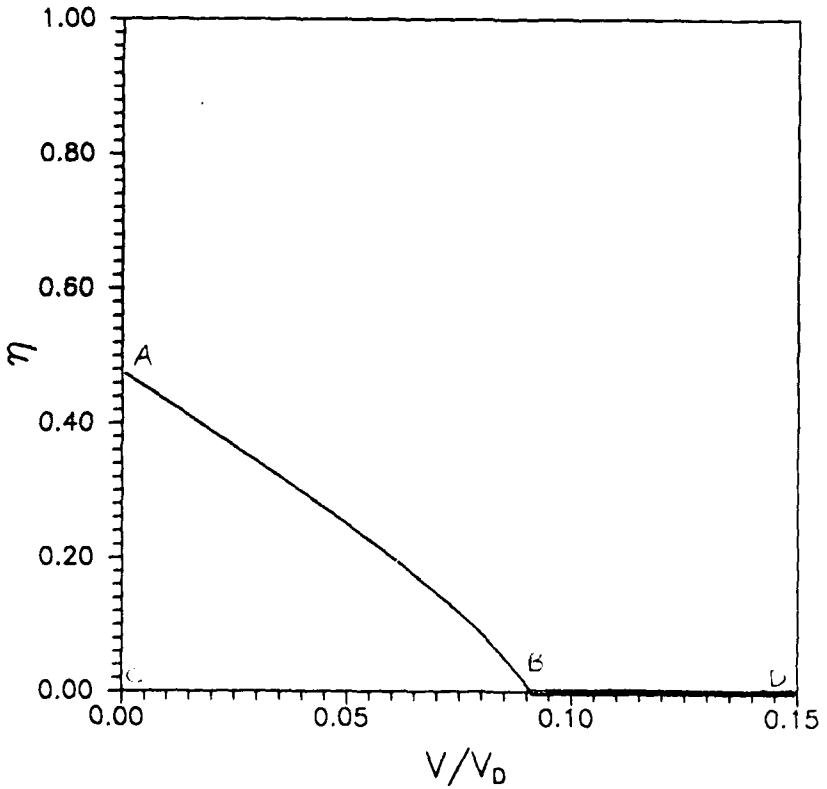
1.00
0.80
0.60
0.40
0.20
0.00
η
A
B
C
D
0.00
0.05
0.10
0.15
V/V_D

(a)

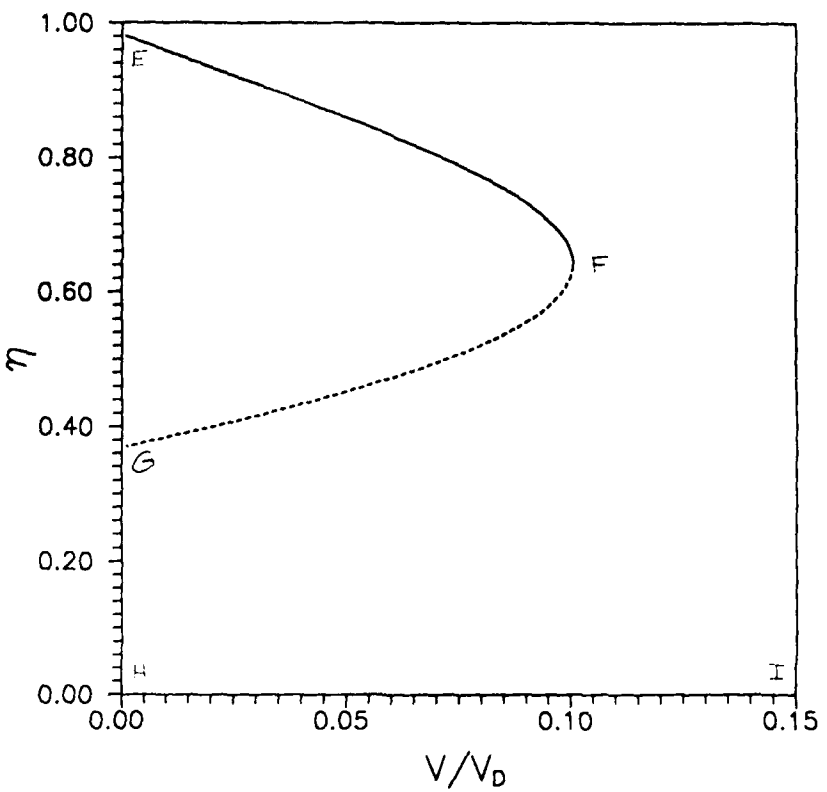
1.00
0.80
0.60
0.40
0.20
0.00
η
E
F
G
H
I
0.00
0.05
0.10
0.15
V/V_D

(b)

Fig 6

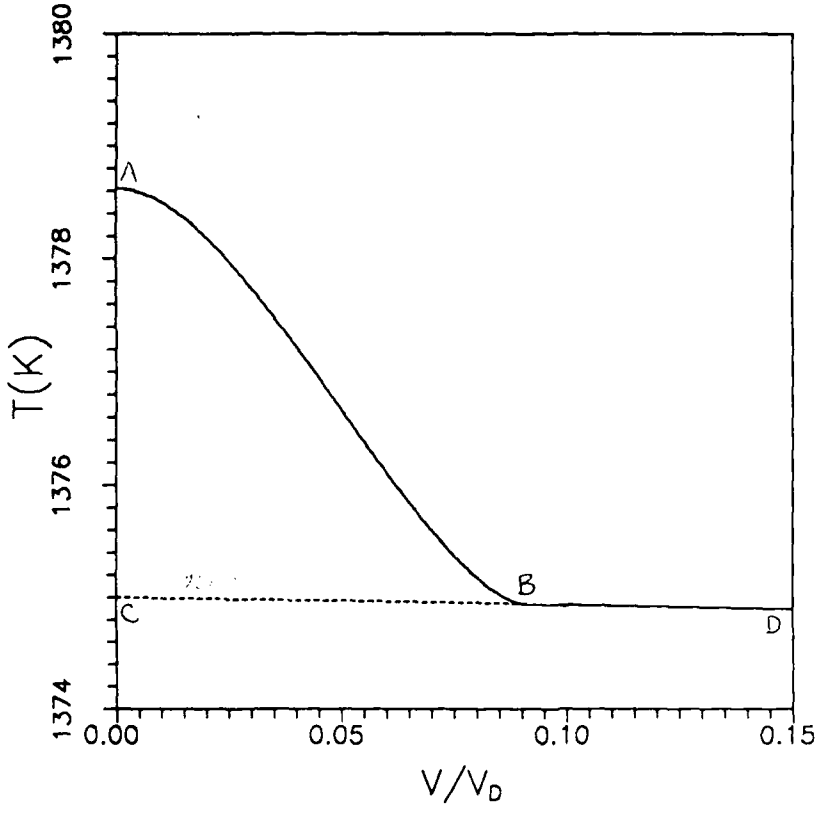
T(K)
1380
1378
1376
1374
A
B
C
D
0.00
0.05
0.10
0.15
V/V_D

(a)

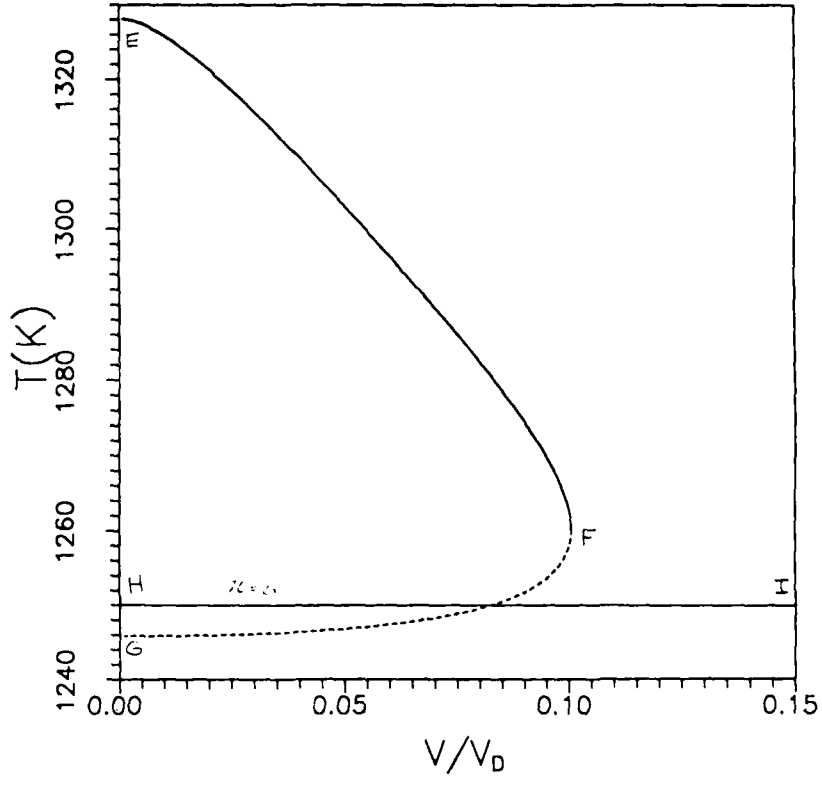
T(K)
1320
1300
1280
1260
1240
E
F
G
H
H
0.00
0.05
0.10
0.15
V/V_D

(b)

Fig 7

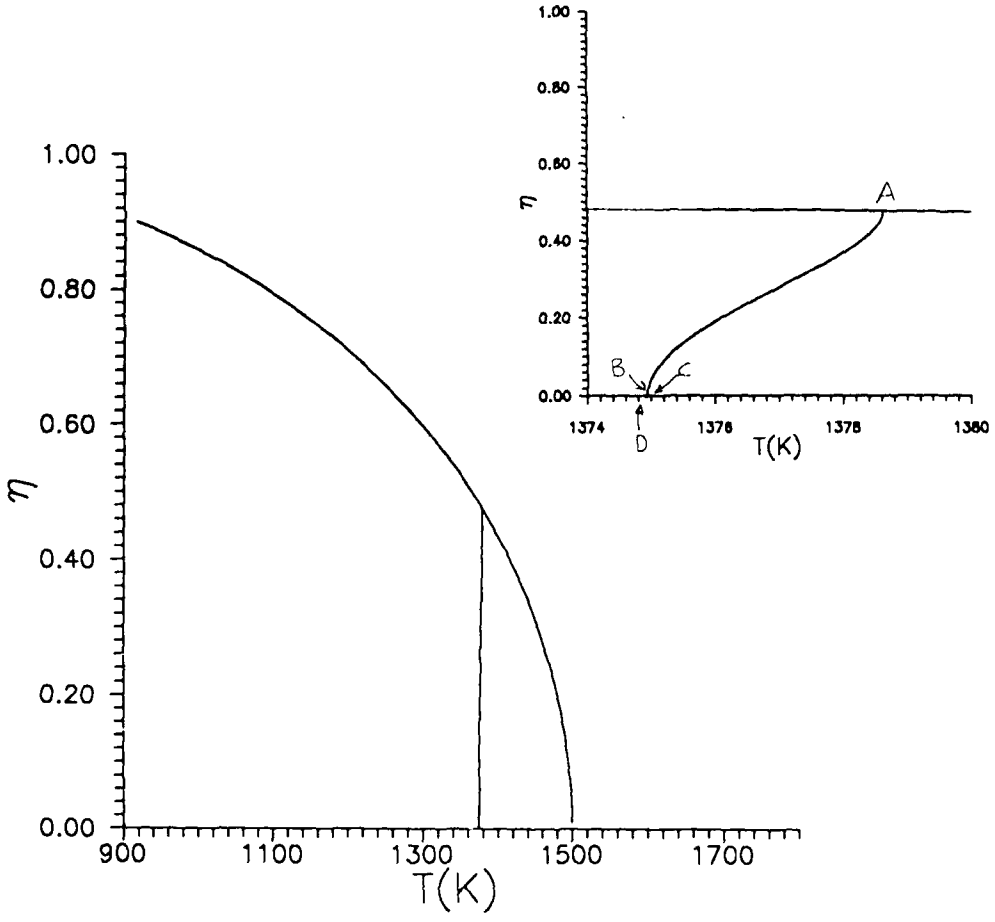
1.00
0.80
0.60
0.40
0.20
0.00
η
900
1100
1300
1500
1700
T(K)
A
B
C
D
1374
1376
1378
1380

Fig 8a

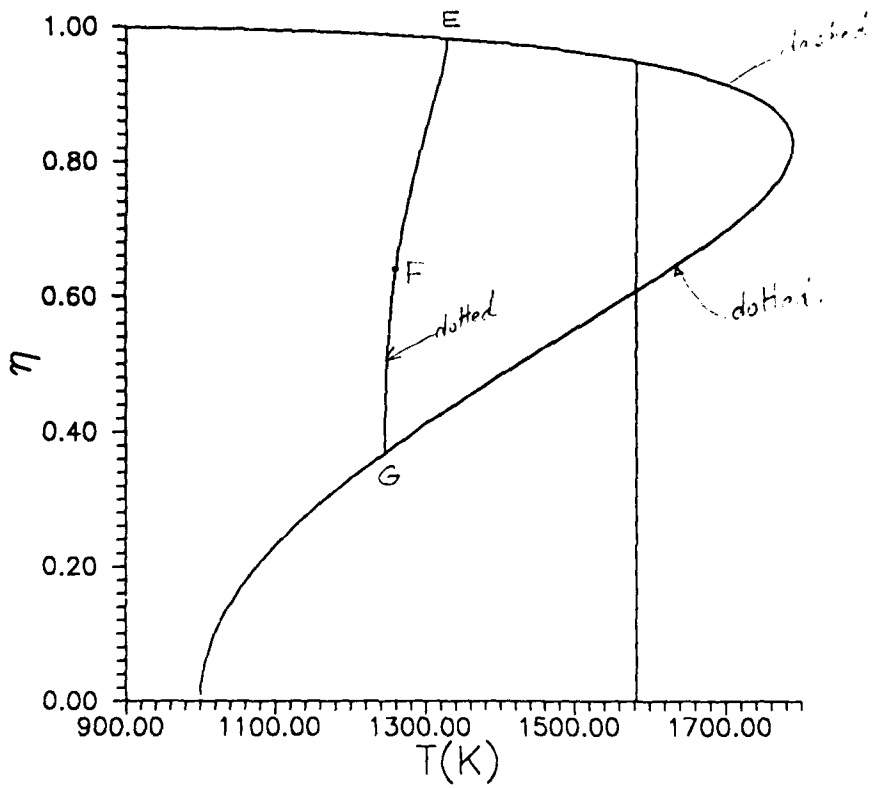
1.00
0.80
0.60
0.40
0.20
0.00
η
E
F
G
dotted
900.00
1100.00
1300.00
1500.00
1700.00
T(K)

Fig 86

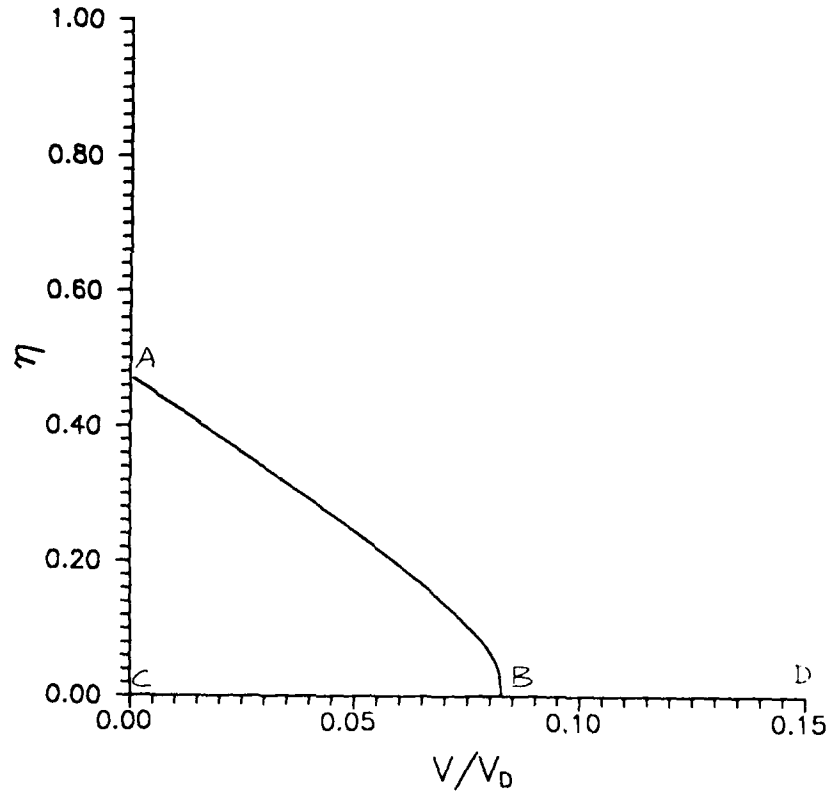

Fig 9a $X_B^S = .48$

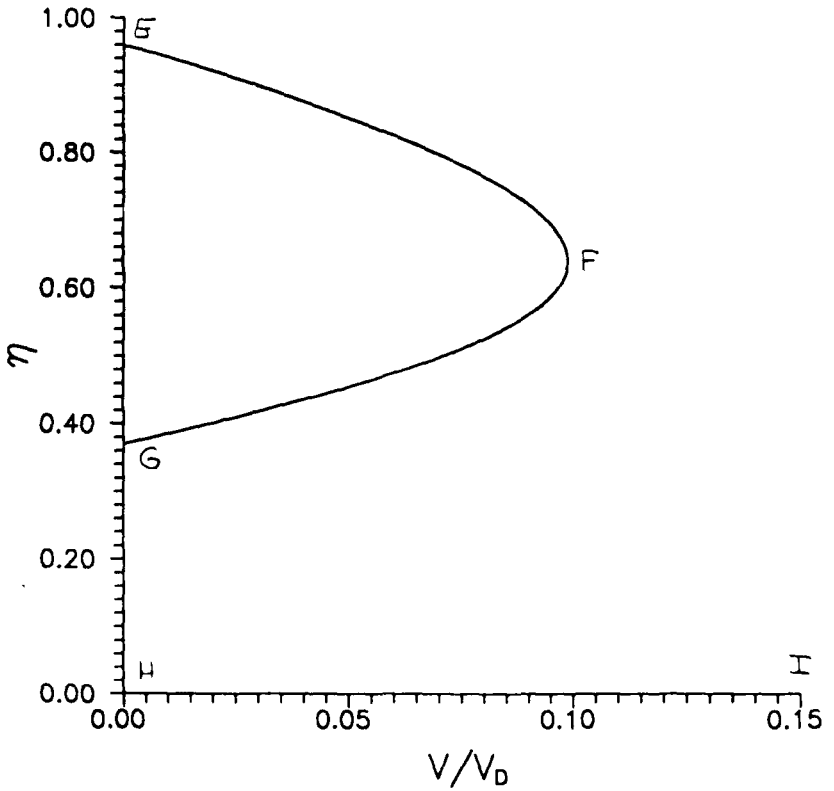

$x_B^S = 0.48$

Fig 9b

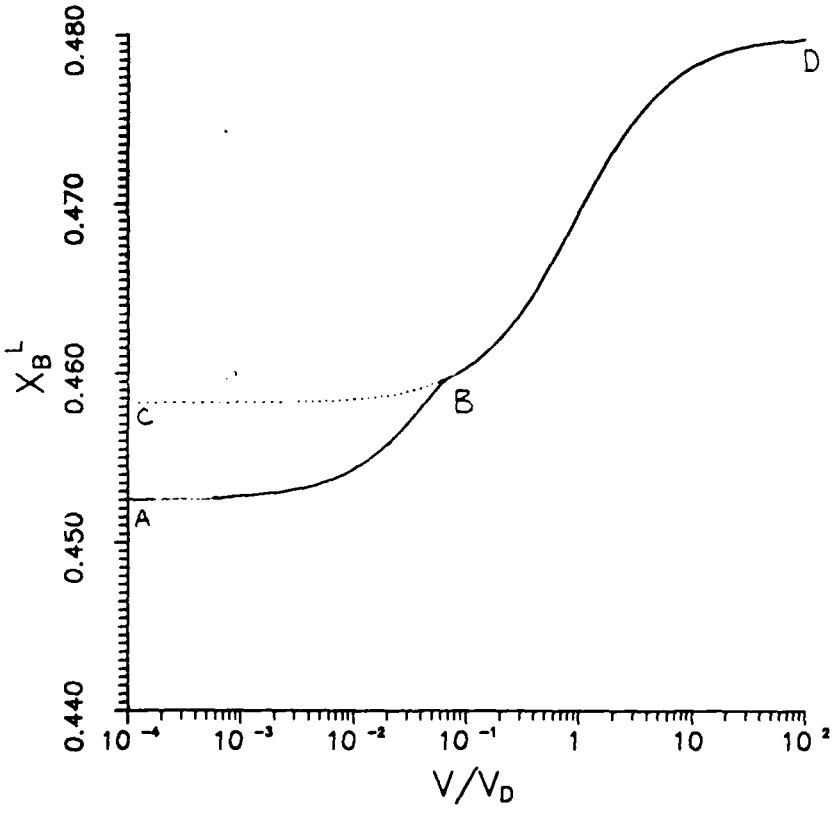
X_B^L
0.480
0.470
0.460
0.450
0.440
A
B
C
D
10^{-4}
10^{-3}
10^{-2}
10^{-1}
1
10
10^2
V/V_D

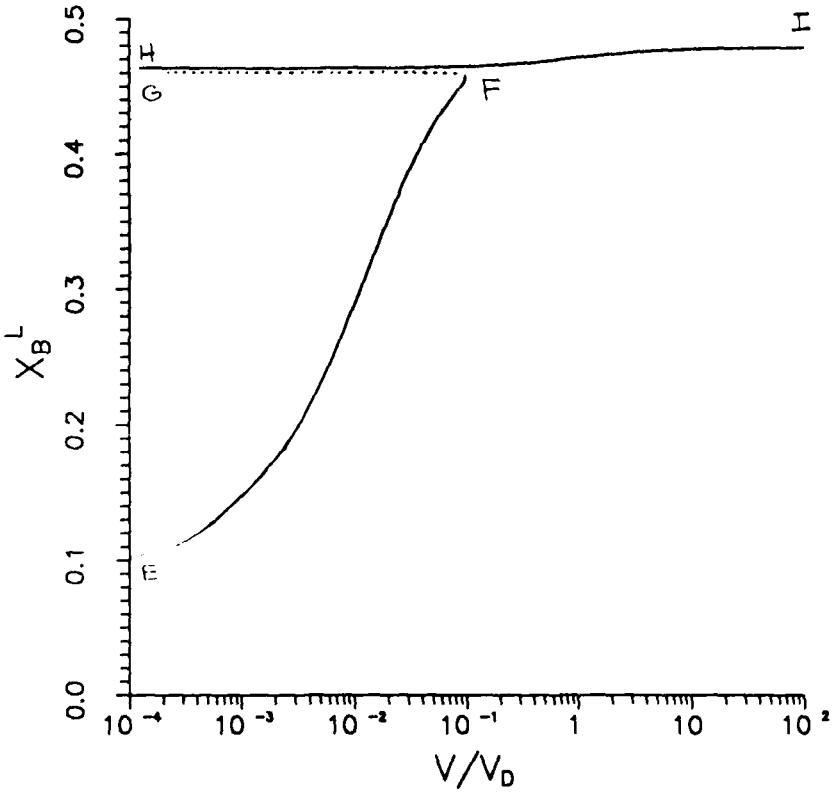
X_B^L
0.5
0.4
0.3
0.2
0.1
0.0
E
F
G
H
H
10^{-4}
10^{-3}
10^{-2}
10^{-1}
1
10
10^2
V/V_D

Fig 10

(a)

(b)